Chemosphere 287 (2022) 132177

Contents lists available at ScienceDirect

Chemosphere

journal homepage: www.elsevier.com/locate/chemosphere

Review

Carbonaceous materials for removal and recovery of phosphate species: Limitations, successes and future improvement

Yasar K. Recepoglu [b], A. Yagmur Goren [c], Yasin Orooji [a,**], Alireza Khataee [d,e,*]

[a] Jiangsu Co-Innovation Center of Efficient Processing and Utilization of Forest Resources, International Innovation Center for Forest Chemicals and Materials, College of Materials Science and Engineering, Nanjing Forestry University, Nanjing, 210037, China
[b] Department of Chemical Engineering, Izmir Institute of Technology, 35430, Urla, Izmir, Turkey
[c] Department of Environmental Engineering, Izmir Institute of Technology, 35430, Urla, Izmir, Turkey
[d] Research Laboratory of Advanced Water and Wastewater Treatment Processes, Department of Applied Chemistry, Faculty of Chemistry, University of Tabriz, 51666-16471, Tabriz, Iran
[e] Department of Environmental Engineering, Gebze Technical University, 41400, Gebze, Turkey

HIGHLIGHTS

- Recent advances on carbon-based materials for phosphate removal and recovery.
- Critical review on activated carbon, carbon nanotube, graphene, gC_3N_4, lignin.
- Comparison of phosphate uptake capacities under optimum experimental conditions.
- Limitations and future aspects of phosphate removal using carbonaceous materials.

GRAPHICAL ABSTRACT

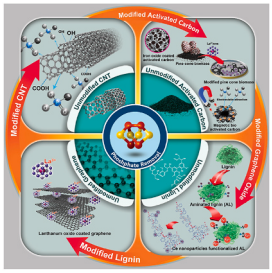

ARTICLE INFO

Handling Editor: Hassan Karimi-Maleh

Keywords:
Phosphate recovery
Activated carbon
Graphene oxide
Lignin
Carbon nanotube
gC_3N_4

ABSTRACT

The carbonaceous materials have gained significant interest for the phosphorus species remediation and recovery in the last decade. Carbonaceous materials present many unique features, such as cost effective, availability, environmentally friendly, and high removal efficiency that make them a promising adsorbent. In this review, the recent application of carbonaceous materials including activated carbon (AC), graphene and graphene oxide (GO), lignin, carbon nanotubes (CNTs), and gC_3N_4 for phosphate removal and recovery were comprehensively summarized. The kinetics and isotherm models, removal mechanisms, and effects of operating parameters are reported. The reusability, lifetime of carbonaceous materials, and impact of modification were also considered. The modified carbonaceous materials have significantly high phosphate adsorption capacity compared to unmodified adsorbents. Namely, MgO-functionalized lignin-based bio-charcoal exhibited a 906.8 mg g^{-1} of capacity as the highest one among other reviewed materials. The modification of carbonaceous materials with various elements has been presented to improve the surface functional groups, surface area and charge, and pore volume and size. Among these loaded elements, iron has been effectively used to provide a prospect for magnetic recovery of the adsorbent as well as increase phosphate adsorption. Furthermore, the phosphate recovery

* Corresponding author.
** Corresponding author. Research Laboratory of Advanced Water and Wastewater Treatment Processes, Department of Applied Chemistry, Faculty of Chemistry, University of Tabriz, 51666-16471, Tabriz, Iran.
E-mail addresses: yasin@njfu.edu.cn (Y. Orooji), a_khataee@tabrizu.ac.ir, akhataee@gtu.edu.tr (A. Khataee).

https://doi.org/10.1016/j.chemosphere.2021.132177
Received 31 July 2021; Received in revised form 26 August 2021; Accepted 3 September 2021
Available online 6 September 2021

methods, phosphate removal efficiency of carbonaceous materials, the limitations, important gaps in the literature, and future studies to enhance applicability of carbonaceous materials in real scale are also discussed.

1. Introduction

Sources of fresh water, such as rivers and lakes, are susceptible to pollutants, and thus, 2.1 billion people suffered from access to safe drinking water owing to a lack of sanitation facilities in different regions of the globe, according to the report of the World Health Organization (WHO) in 2018 (WHO, 2018). The ever-increasing levels of phosphorus in water bodies pose most pollution problems that include harming water quality, food resources and habitats, and decreasing oxygen level for marine life (Nakarmi et al., 2020). Since phosphate is a non-renewable inorganic salt that is used in fertilizers to meet the demand for agricultural supplies by increasing the production yield of crops, phosphorus pollution has become one of the significant environmental concerns due to a dramatic increase in discharges from agricultural runoff, urbanization, and industrial activities. Even though phosphorus is a vital nutrient for plant growth and evolution, it can accelerate algal blooms and cause eutrophication when the amounts of phosphate exceed 25 μg L^{-1} in surface water. Eutrophication resulted from algae overgrowth can threaten human health, destroy the self-purification capacity of water, cause detrimental effects to aquatic systems, and lower water quality (Buates and Imai, 2020; Mohammadi et al., 2021; Yin et al., 2018; Zhang et al., 2019b. In fact, water becomes polluted and useless due to the simple oxidation of organisms and dead algae in the water (Wang et al., 2020). Thus, effective control of phosphate application has been attracting a great deal of attention over the last years. Moreover, the sustainable management of phosphate play an important role in terms of environmental and economical perspective. Phosphate is widely gained from naturally phosphate containing rocks, but phosphate reserves are located in number of countries like China, Morocco, and the US (Smol, 2019). Besides, the phosphate rock is classified as a critical raw material for production of phosphate containing fertilizers and feed considering increasing population (Mathieux et al., 2017). Therefore, the phosphate recovery technologies have been gained significant attention to recover phosphate and reuse it industrial and agricultural purposes. The most significant sources of phosphate are secondary sources such as industrial wastewater, municipal wastewater, sewage sludge, and biomass ash (Sarvajayakesavalu et al., 2018). In this perspective several technologies investigated for phosphate recovery and removal.

Precipitation with chemicals such as aluminum, calcium, and iron salts, is one of the techniques that is practically applied as a traditional method for the removal and recovery of phosphate in an aqueous medium. Calcium oxide/hydroxide is not often preferred despite being low-cost and effective precipitant for phosphate in wastewater because the pH level must be around 9.5–10 for precipitation to occur and then must be lowered to a suitable level before being discharged into waterways. On the other hand, if trivalent cations such as aluminum and iron are used, a metal phosphate sludge is generated, often resulting in the recovery problem. Thereby, secondary waste disposal issues become inevitable as long as removed phosphate is directly discarded with generated sludge as waste without recovery (Diamadopoulos and Benedek, 1984; Labgairi et al., 2020; Luedecke et al., 1988). Notable drawbacks of the chemical precipitation method have restricted extensive application and have forced the development of alternative processes. One of such methods is microbial digestion, where microorganisms are fed on phosphate, and other nutrients exist in the wastewater. Although the resulting digestate can be used as inorganic fertilizer, this method requires strictly controlled conditions to maintain appropriate discharge limits. Otherwise, any disturbance in process inputs such as improper handling of the resulting sludge or low carbon may release phosphorous into wastewater streams rather than capturing (Marshall et al., 2017). The other strategy to reduce phosphorus content in wastewater effluent is retrofitting the being present plants for improved removal of phosphorus with biologically (EBPR), which depends on the potential of used microorganisms to remove phosphate from the aqueous environment and convert it to the solid environment in the form of intracellular poly-phosphate. Nevertheless, EBPR in full-scale systems can generate effluent with as low as 0.1 mg L^{-1} of phosphorus concentrations, reliably meeting low effluent limits, and troubleshooting treatment upsets can be difficult (R. Liu et al., 2019). Another alternative method for phosphate removal is adsorption. A variety of studies have been reported for phosphate removal using materials such as natural products, by-products, and synthetic products. However, many of them have either insufficient phosphate adsorption capacities or toxic leach compounds such as heavy metals into the environment (Veni et al., 2017). The precursors for the prepared or used adsorbents should be bio-compatible, bio-degradable, easily available, eco-friendly, and possess high adsorption capacities such as carbonaceous materials (Hassani and Khataee, 2021; Kalderis et al., 2020; Khataee and Hasanzadeh, 2017). As a result, studies have concentrated on the use of carbonaceous materials for phosphate removal. Although there are some novel applications of carbon-based materials like electrochemical sensor (Sarıoğulları et al., 2019), antifouling and improved desalination performance in membranes (Safarpour et al, 2015, 2016), various carbonaceous materials, like activated carbon (AC), biochar, carbon nanotubes (CNTs), graphene, graphene oxide (GO), gC_3N_4, lignin, and other unclassified carbonaceous materials have been traditionally used for phosphate removal as well (Al-Zboon, 2018; Mekonnen et al., 2020). The chemical and physical relations between phosphate and carbonaceous materials control the removal of phosphate in water sources. Electrostatic interaction, ion exchange, precipitation, Lewis's acid-base interactions, and hydrogen bonding are some of the dominant mechanisms reported for the adsorption of phosphate ions onto these adsorbents. The possible reactions between aluminum-magnesium modified carbonaceous material and phosphate in water are given in Fig. SM1. In this context, the current review collects a critical and comprehensive literature survey that includes recent advances for the removal and recovery of phosphate using carbonaceous materials. A summary of the reported studies in terms of preparation and characterization of the materials, optimum adsorption conditions, isotherms, kinetics, and maximum adsorption capacity are presented in detail. Furthermore, the limitations and the future aspects of phosphate remediation by carbonaceous materials are also highlighted.

2. Activated carbon

2.1. Unmodified activated carbon without further modification

AC is a versatile adsorbent with high adsorption capacity depending on its high surface area and porous nature with a standard application in water purification to remove organic and inorganic pollutants (Hassani and Khataee, 2017; Orooji et al., 2021). AC can be manufactured from several biomass or fossil-based feedstock such as banana waste, coconut shell, rice husk, and coal (Kalderis et al., 2008; Khataee, A.R., Aber, S., Zarei, M., Sheydaei, 2011). There are also many studies about the preparation of AC from different waste materials, e.g., cherry stones and peanut husk (Table SM1). The preparation of carbon adsorbents is generally energy-intensive that leads to high prices in commercial AC. Fundamentally, there are two different processes for the preparation of AC, including physical and chemical activation. Physical activation can be done, for example, with CO_2 or thermal treatment. In contrast, in chemical activation, different chemical activating agents that are

typically alkali and alkaline earth metals containing substances such as KOH, NaOH, and $ZnCl_2$ or some acids such as H_3PO_4 is used (Kilpimaa et al., 2014).

Namasivayam and Sangeetha (2004) developed AC from coir pith using $ZnCl_2$ for chemical activation to remove phosphate from water. Langmuir adsorption capacity was 5.1 mg g^{-1}, and the removal was maximal in the pH range 3–10. Adsorption of phosphate followed pseudo-second-order (PSO) kinetics (k_2 = 0.188 g $(mg.min)^{-1}$). Coir-pith AC (CAC) was also prepared by sulfuric acid as a chemical activating agent and employed to remove phosphate ions from aqueous solutions. Equilibrium was attained after 3 h, and 7.56 mg g^{-1} of maximum adsorption capacity was calculated from Langmuir isotherm model at pH of 6, adsorbent dose of 4 g L^{-1}, and 333 K (Kumar et al., 2010). Xu et al. (2015) prepared *Arundo donax* Linn-based resin (ADI-resin) and *Arundo donax* Linn-based activated carbon (ADI-AC) and compared their phosphate elimination efficiency from water. Although the BET surface area of ADI-AC was higher with 1034 m^2 g^{-1} than that of ADI-resin (8.4 m^2 g^{-1}), the phosphate adsorption capacity was 7.7 mg g^{-1} and 65.3 mg g^{-1}, respectively. Kilpimaa et al. (2015) prepared an adsorbent by physical activation of carbon residue obtained as a by-product from wood gasification process with 590 m^2 g^{-1} of BET surface area. They found Langmuir adsorption capacity of 30.211 mg g^{-1} under optimal conditions that are pH of 6 and initial concentration of 20 mg L^{-1}. Mor et al. (2017) compared commercially available activated charcoal with nano-alumina for phosphate removal. The highest removal efficiency of 90.2% was observed in reaction time of 120 min at pH of 4 and 30 °C with 3.2 g L^{-1} of dosage by activated charcoal, whereas 100% removal was obtained at pH of 2, temperature of 40 °C with nano-alumina at 90 min using 1.6 g L^{-1} of adsorbent dose. As the best-fitted isotherm, the Langmuir model revealed 0.461 mg g^{-1} and 0.165 mg g^{-1} of adsorption capacities for activated charcoal and nano-alumina, respectively. AC was derived from *Prosopis juliflora* (PJAC) to evaluate its phosphate reduction in single and multi-component water medium. Among other components such as metronidazole and nitrate in the solution, phosphate removal was the highest as 15.2 mg g^{-1} by PJAC. In contrast, it was 13.55 mg g^{-1} in a single-component system (only phosphate), attributing to improved adsorption efficiency (Manjunath and Kumar, 2018). Astuti et al. (2019) prepared a series of ACs from the teak leaf using both microwave irradiation and furnace heating with $ZnCl_2$ of 20% and 30% by mass for chemical activation. The results showed that microwave heated AC with 30% $ZnCl_2$ had the highest BET surface area of 219.79 m^2 g^{-1} leading to the best phosphate adsorption efficiency at the optimum conditions, pH of 4 and equilibrium time of 180 min with 85.47 mg g^{-1} of adsorption capacity. Langmuir equilibrium model (K_L = 24.372 L mg^{-1}) and PSO kinetic model (k_2 = 0.0041 g $(mg.min)^{-1}$) described the adsorption of phosphate by teak leaf activated carbon. ACs prepared from oily sludge through physical and chemical activation were utilized to remove phosphate from aqueous solutions. The optimum adsorbent was obtained via $ZnCl_2$ activation at 500 °C with a BET surface area of 1259 m^2 g^{-1} and a maximum phosphate adsorption capacity of 102 mg g^{-1} adsorbent dose of 1 g L^{-1} and pH of 6 (Mojoudi et al., 2019). Sreekumar et al. (2019) prepared an AC from wasted sludge and compared its efficiency with thermally treated laterite soil (TAL) to abate phosphate from synthetic wastewater. AC exhibited better adsorption performance with 0.795 mg g^{-1} of capacity than TAL with 0.690 mg g^{-1}. Recently, *Glycyrrhiza glabra* residue-based AC prepared by loading of $ZnCl_2$ with a surface of 959.22 m^2 g^{-1} was operated for phosphate removal via batch studies. The highest capacity activated carbon was estimated to be 92.5 mg g^{-1} by the Langmuir model fitted with experimental data satisfactorily. Batch studies revealed an optimum adsorbent dosage of 6 g L^{-1} (Najmi et al., 2020). Miyazato et al. (2020) tested nine commercial ACs mainly derived from coconut shells and the rest from coal, sawdust, and petroleum resin to recover phosphate. AC with the name of AC-Naca-Coal having BET surface area of 859 m^2 g^{-1} had the highest adsorption capacity, 5.4 mg g^{-1}, among others at 303 K, but it also exhibited the largest one meaning that the amount of potentially recoverable phosphate ion by the temperature swing between 303 and 373 K is low. Overall, the main kinetic and adsorption models was reported to be PSO and Langmuir, respectively. The Langmuir model rate constant was found to be in the range of 0.009–1428 L mg^{-1}, while the PSO kinetic constant was in the ranege of 0.0041–0.188 g $(mg.min)^{-1}$. The adsorption capacities were found to be in the range of 0.69–102 mg g^{-1} at optimum pH value of 6.

2.2. Modified activated carbon

Modified AC samples are carbonaceous materials with some specific intercalating groups immobilized at their surface to further improve the recyclability and adsorption efficiency. Several modification techniques were used to enhance adsorption, adsorption capacity and improve carbon selectivity (Monser and Adhoum, 2002). Many studies on the evaluation of phosphate adsorbents have successfully brought about various modification agents such as aluminum hydroxide and oxides, iron oxides, lanthanum (hydr)oxides, and layered double hydroxides (LDHs). The combination of AC and modification agent loading could proceed advantage of the strength of these developed materials. While the AC serves as a perfect support media for modifiers, the preloaded modifier offers a higher affinity for phosphate in the solution. The literature on phosphate removal from aqueous solutions using modified AC adsorbent is summarized in Table 1. Several elements, including Zr, Fe, La, and Ca, were used in modification of adsorbents to optimize the phosphate removal performance. The kinetics and isotherms models were also considered, and the results presented that PSO and Langmuir, respectively, commonly followed the kinetic and isotherm models.

Yao et al. (2018) prepared ACs from sewage sludge by chemical activation with pyrolusite (PAC) to develop a promising adsorbent for phosphate removal from an aqueous solution. Despite its relatively lower maximum adsorption capacity (10.78 mg g^{-1}), good performance with a high phosphate removal rate (ca. 90%) in a wide pH range (4–8) within 30 min was reported. Cork powder-based AC stabilized nano-zero-valent iron (AC/NZVI) composite was developed and tested for efficient phosphate removal. Process parameters were optimized using response surface methodology with Box-Behnken resulting in a pH of 3.5, a temperature of 60 °C, and an AC/NZVI dosage of 0.4 g L^{-1}. Under the optimum conditions, 151.10 mg g^{-1} of adsorption capacity was obtained for an initial phosphate concentration of 211 mg L^{-1} (Singh and Singh, 2018). Makita et al. (2019) prepared a composite from commercially available granular AC by loading metal-oxides such as lanthanum, cerium, or iron oxide onto it and compared their phosphate removal performances. The phosphate adsorption was obtained as in the order of iron oxide- < cerium oxide- < lanthanum oxide-loaded carbonaceous materials corresponding to 17, 44, and 72 mg per gram of the loaded metal oxide. Polyacrylonitrile-based carbon fiber (PAN-CF) was activated with K_2CO_3 and heat treatment at 950 °C for phosphate removal from an aqueous solution. A maximum adsorption capacity of 64.58 mg g^{-1} was determined from the Langmuir model (K_L = 0.321 L $mmol^{-1}$), and a relatively high adsorption rate to reach equilibrium (<1 h) was observed for this adsorbent as well (Sakamoto et al., 2020). Han et al. (2020) developed magnetic bio-ACs (MBACs) from mixing lignin with ferrous salt via carbonization followed by steam activation to remove phosphate from aqueous solutions. Surface modification of AC derived from lignin with iron enhanced the maximum adsorption capacity and was estimated to be 21.18 mg g^{-1}. Magnetization of AC derived from banana bract and further crosslinking of amine groups was performed to prepare an efficient adsorbent called ACM@BBAC to recover phosphate and nitrate ions from water (Fig. 1(a)). The effects of operating parameters including reaction time (0–90 min), adsorbent dose (0.5–4 g L^{-1}), and pH (2–12) on phosphate removal performance of advanced material were investigated. Furthermore, the synthesized material's magnetic property was investigated with VSM analysis, and the magnetization curve of the material was S-shape representing super

Table 1
Summary of the literature studies on recovery of phosphate with different modified activated carbon.

Adsorbent	Activated carbon source	Modification agent	Surface area (m^2 g^{-1})	Adsorption capacity (mg g^{-1})	Isotherm constant (L mg^{-1})	Kinetic (mg (g.min)$^{-1}$)	Optimum conditions	Reference
Zirconium loaded activated carbons	Rice straws Cedar bar Waste cardboard sludge	$ZrNO_3$	623 743 394	11.1 3.83 5.97	5.08^{L} 0.393^{L} 1.43^{L}	$N.A.^{PSO}$	Adsorbent dose: 10 g L^{-1}, T = 25 °C, pH < 9	Shindo et al. (2011)
Lanthanum-doped activated carbon fiber	Commercial	$LaNO_3$	N.A.	9.41	3.52^{L}	0.01^{PSO}	Adsorbent dose: 2 g L^{-1}, T = 50 °C, pH = 4	Liu et al. (2011)
Iron-doped activated carbon	Commercial	$FeSO_4{\cdot}7H_2O$ $FeCl_3{\cdot}6H_2O$	880.65 302.61	14.12 8.13	1.85^{L}	0.011^{PSO}	Adsorbent dose: 2 g L^{-1}, T = 25 °C, pH = 3.78–6.84	Wang et al. (2012)
Lanthanum hydroxide-doped activated carbon fiber	Commercial	$LaNO_3$ and NaOH	N.A.	15.3	1.43^{L}	0.002^{PSO}	Adsorbent dose: 2.5 g L^{-1},T = 25 °C,pH < 10.0, Equilibrium time: 6 h	Zhang et al. (2012b)
Lanthanum-doped activated carbon fiber	Commercial	$LaNO_3$	1047.86	7.46	3.45^{L}	0.017^{PSO}	Adsorbent dose: 2 g L^{-1}, T = 30 °C	Zhang et al. (2012a)
Hydroxyl-iron-lanthanum doped activated carbon fiber	Commercial	N.A.	N.A.	29.44	8.60^{L}	0.037^{PSO}	Adsorbent dose: 1 g L^{-1}, T = 25 °C, pH = 4	Liu et al. (2013)
Iron containing non-oxidized and oxidized activated carbons	Commercial	HNO_3 and $FeSO_4$ $FeSO_4$	1059.67 880.65	7.46 13.12	0.25^{L} 0.62^{L}	0.016^{PSO} 0.017^{PSO}	Adsorbent dose: 2 g L^{-1}, T = 30 °C	Wang et al. (2014)
Zirconium-loaded activated carbon	Commercial	$ZrNO_3$	N.A.	60.78	1.32^{L}	N.A.	Adsorbent dose: 5 g L^{-1}, T = 25 °C, pH≤6	Wajima (2016)
Nano-scale zero-valent iron supported on treated activated carbon	Activated carbon norit	$FeCl_3{\cdot}6H_2O$	740	1.75	1.509^{L}	N.A.	N.A.	Khalil et al. (2017)
Iron nano-magnetic particle coated with powder activated carbon	Commercial	N.A.	N.A.	3.48	0.571^{F}	$N.A.^{PSO}$	Adsorbent dose: 1 g L^{-1}, T = 25 °C, pH = 2, Equilibrium time: 90 min	Khodadadi et al. (2017)
Calcium alginate beads doped with active carbon derived from *A. aspera* plant	*Achyranthes aspera* plant	Ca alginate beads	N.A.	133.3	1.466^{L}	0.419^{PSO}	Adsorbent dose: 1.5 g L^{-1},T = 30 °C,pH = 10, Equilibrium time: 20 min	Sujitha and Ravindhranath (2017)
Iron-zirconium modified activated carbon nanofiber	Commercial	$ZrOCl_2$ and $FeNO_3$ mixture	N.A.	26.3	1.206^{L}	0.005^{PSO}	Adsorbent dose: 3 g L^{-1}, T = 25 °C, pH = 4	Xiong et al. (2017)
Iron oxide coated granular activated carbon	Commerical (supplier: Norit) Commerical (supplier: Desotech) Commerical (supplier: Mast Carbons)	$FeCl_3.6H_2O$	920 441 794	10.4 10.8 10.8	0.05^{L} 0.13^{L} 0.25^{L}	0.0004^{PSO} 0.00028^{PSO} 0.00088^{PSO}	Adsorbent dose: 2 g L^{-1}, T = 22 °C, pH = 6.5	Kumar et al. (2017)
Chitosan and activated carbon nanocomposite	Palm kernel	Chitosan gel	N.A.	6.14	N.A.	N.A.	Adsorbent dose: 3.33 g L^{-1}, T = 25 °C,pH = 7, Equilibrium time: 60 min	Rezaei et al. (2019)
Lanthanum-modified activated carbon	Pine cone	$LaCl_3$	380.4	68.2	0.02^{L}	$N.A.^{PSO}$	Adsorbent dose: 1 g L^{-1}, T = 20 °C, pH = 6–7, Equilibrium time: 90 min	Huong et al. (2019)
Zirconium chloride octahydrate/ cetyltrimethylammonium bromide/vetiver grass-activated carbon	Vetiver grass	$ZrCl_4$ and $C_{19}H_{42}BrN$	222.95	4.27	0.00234^{F}	0.138^{PSO}	Adsorbent dose: 6 g L^{-1}, T = 25 °C, pH = 2–10, Equilibrium time: 120 min	(J. Li et al., 2020)
Coconut shell activated carbon oxidized with HNO_3 and modified with iron	Coconut shell	$FeCl_3{\cdot}6H_2O$	604.88 $Å^2$	14.78	0.00407^{F}	0.001^{PSO}	Adsorbent dose: 2 g L^{-1}, T = 30 °C, pH = 2	Delgadillo-Velasco et al. (2021)

*N.A: Not available, L: Langmuir isotherm, F: Freundlich istotherm, PSO: Pseudo second-order.

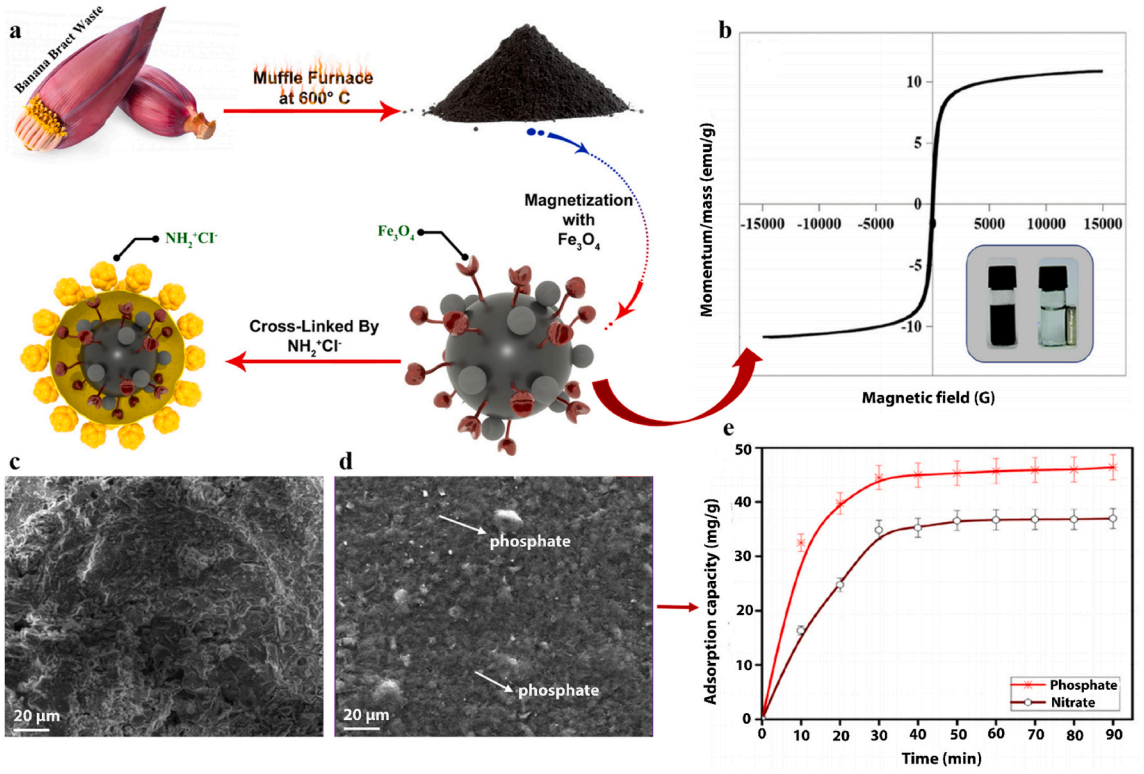

Fig. 1. (a) Preparation of amine crosslinked magnetic banana bract activated carbon (ACM@BBAC) adsorbent, **(b)** VSM analysis of ACM@BBAC adsorbent, **(c)** SEM of AC, **(d)** SEM of phosphate loaded ACM@BBAC, and **(e)** Phosphate and nitrate adsorption capacity of ACM@BBAC (initial phosphate: 100 mg L^{-1}, adsorbent dose: 2 g L^{-1}, pH:7). Adapted from [Karthikeyan and Meenakshi, 2020] with permission from Elsevier (License number: 5070320223209).

magnetic feature (Fig. 1(b)). The material's surface morphology was also presented with SEM images before and after phosphate adsorption experiments (Fig. 1(c)–(d)). The phosphate and nitrate adsorption capacity increased with increasing reaction time from 0 to 30 min with superfast adsorption performance (Fig. 1(e)). ACM@BBAC exhibited superior properties and 91.78 mg g^{-1} of adsorption capacity that can be considered promising for field applications (Karthikeyan et al., 2020b). Moreover, banana bract-based AC was employed to synthesize a composite material containing LDHs of the binary composite ZnAl LDHs co-precipitation technique in another study. As the temperature increased from 303 K to 323 K, the adsorbent's phosphate adsorption capacity increased from 87.004 to 88.121 mg g^{-1}, which perfectly agreed with the endothermic nature of the process (Karthikeyan and Meenakshi, 2019). Karthikeyan and Meenakshi (2020) also synthesized ZnFe LDHs impregnated orange peels AC (OPAC) composite by ultrasound-assisted method for the removal of phosphate from aqueous solutions. Eco-friendly and cost-effective adsorbent showed 84.51 mg g^{-1} of adsorption capacity and followed PSO ($k_2 = 0.412$ g (mg.min)$^{-1}$) and intra-particle diffusion kinetics. Another modified AC was synthesized from a combination of Muskmelon Peel-based AC and zinc ferrite ($AC@ZnFe_2O_4$) by co-precipitation method for removing phosphate from water. With 91.80 mg g^{-1} of adsorption capacity at 30 °C, it possessed a remarkable efficiency among its counterparts (Karthikeyan et al., 2020a). Silver nanoparticles loaded AC produced from tea residue (AgNPs-TAC) material was used for phosphate removal from the aqueous solution with an initial phosphate concentration of 30 mg L^{-1}. Optimal conditions were determined as pH of 3, contact time of 150 min, and impregnation ratio (AgNPs/TAC) of 3% w/w that resulted in 13.62 mg g^{-1} of maximum adsorption capacity. Both pseudo-first-order and PSO kinetic models described adsorption models attributing to chemisorption for the rate control step (Nguyen et al., 2020).

The phosphate adsorption capacities and dosages of zirconium loaded AC from cedar bar (Zr-CB-AC) and rice straw (Zr-RS-AC), zirconium chloride octahydrate-cetyltrimethylammonium bromide-vetiver grass-AC (ZR-CTB-VG-AC), iron containing AC (Fe-AC), lanthanum-doped AC fiber (La-ACF), iron oxide coated granular AC (Fe-GAC), iron loaded AC from coconut shell (Fe-CS-AC), lanthanum hyrdoxide-doped AC fiber (LaOH-ACF), iron-zirconium modified AC nanofiber (Fe–Zr-ACNF), iron-lanthanum doped AC fiber (Fe–La-ACF), zirconium-loaded AC (Zr-AC), lanthanum-modified AC (La-AC), and calcium alginate beads doped with AC derived from *A. aspera* plant (CAB-AP-AC) were reported in Table 1 and presented in Fig. SM2. The operating conditions are varying from 1.0 to 10 g L^{-1} for the adsorbent dose, from 20 °C to 50 °C for the temperature, from 2 to 10 for the pH and from 20 min to 6 h for equilibrium time. The calcium alginate beads doped with AC derived from *A. aspera* plant (CABAA) showed the highest phosphate adsorption capacity of 133.3 mg g^{-1} with low adsorbent dosage of 1.5 g L^{-1} compared with other AC based materials. Furthermore, lanthanum-modified AC-based materials achieved relatively higher phosphate adsorption capacity than iron-modified materials due to its higher phosphate adsorption afinity.

3. Graphene and graphene oxide (GO)

Graphene has an entire structure and unique electronic features, which have gained significant attention from scientists (Wang et al., 2011). GO, a precursor for graphene preparation, is a promising and valuable material for applications in electronics, optics, chemistry, energy storage, and biology (Cha-Umpong et al., 2019; Heidarizadeh et al., 2017; Razmjou et al., 2020; Rostamnia et al., 2015). Furthermore, graphene and GO were operated as adsorbents to remove arsenic, fluoride, methyl orange, naphthalene, heavy metals in waters and presented good adsorption efficiency and superfast adsorption rates (Fakhri, 2017; Hassandoost et al., 2019; Safarpour and Khataee, 2019). The literature on removing phosphate in aqueous environments using modified graphene and GO adsorbent is summarized in Table 2. Several

Table 2
Summary of the literature studies on recovery of phosphate with different modified graphene-graphene oxide.

Adsorbent	Modification agent	Surface area (m^2 g^{-1})	Adsorption capacity (mg g^{-1})	Isotherm constant (L mg^{-1})	Kinetic (mg $(g.min)^{-1}$)	Optimum conditions	Removal mechanism	Reference
Ferrihydrite loaded on the graphene oxide composite	$5Fe_2O_3.9H_2O$	N.A.	5.81	2.14^{L}	N.A.	Adsorbent dose: 1.33 g L^{-1}, T = 25 °C, pH = 2, Equilibrium time: 500 min, $C_{phosphate}$: 5 mg L^{-1}	N.A.	(X. Li et al., 2020)
Zirconium-loaded reduced graphene oxide	$C_{12}H_{28}O4Zr$	251.1	27.71	17.19^{L}	0.11^{PSO}	Adsorbent dose: 0.2 g L^{-1}, T = 25 °C, pH = 5	Ion exchange and ligand exchange (outer or inner sphere complexes) and physical adsorption	Luo et al. (2016)
Graphene Oxide Decorated with α-Fe_2O_3	$FeCl_3{\cdot}6H_2O$	N.A.	93.28	0.5129^{L}	0.0555^{PSO}	Adsorbent dose: 0.65 g L^{-1}, T = 25 °C, pH = 6, Equilibrium time: 5 min, $C_{phosphate}$: 50 mg L^{-1}	Electrostatic attraction and ion exchange reaction	Bai et al. (2018)
Graphene–nanoparticle aerogel composite decorated with magnetit	$FeSO_4$	130	350	9.96^{F}	0.005^{PSO}	Adsorbent dose: 0.2 g L^{-1}, T = 25 °C, pH = 6, Equilibrium time: 120 min, $C_{phosphate}$: 20 mg L^{-1}	Mononuclear and polynuclear adsorption	Tran et al. (2015)
Reduced graphene oxide -coated ZnO and Fe hybrid nanocomposite	$FeNO_3$ and $ZnNO_3$	103.7	N.A.	N.A.	N.A.	Adsorbent dose: 0.1 g L^{-1}, T = 160 °C, Equilibrium time: 48 h	N.A.	Lee et al. (2020)
Triethylene Tetramine Functionalized Magnetic GO Chitosan Composite	$FeCl_3{\cdot}6H_2O$ and $FeCl_2{\cdot}4H_2O$	131.5	353.36	0.027^{L}	0.0018^{PSO}	Adsorbent dose: 0.4 g L^{-1}, T = 25 °C, pH = 3, Equilibrium time: 50 min	Electrostatic interaction	(H. Wang et al., 2017)
La(III) coagulated graphene oxide	N.A.	N.A.	141.38	3.39^{L}	$N.A.^{PSO}$	pH= >7, Equilibrium time: <20 min	Surface binding	Chen et al. (2017)
Zirconium functionalized nanochitosan- graphene oxide composite	$ZrCl_4$	118.45	172.41	21.02^{F}	0.0008^{PSO}	Adsorbent dose: 0.5 mg L^{-1}, T = 25 °C, pH = 3, $C_{phosphate}$: 30 mg L^{-1}	Coordination and electrostatic interaction	Salehi and Hosseinifard (2020)
Surface-imprinted polymer by developing a La(III)-coordinated 3-methacrylox-yethyl-propyl bi-functionalized graphene oxide	N.A.	N.A.	104.3	0.1304^{L}	0.1189^{PSO}	Adsorbent dose: 0.4 g L^{-1}, T = 25 °C, pH = 3, Equilibrium time: 40 min	Ligand exchange and electrostatic repuslsion	Liu et al. (2018)
Strontium magnetic graphene oxide nanocomposite	$SrNO_3$	N.A.	238.09	0.33^{L}	0.00005^{PSO}	Adsorbent dose: 30 mg, T = 25 °C, pH = 6, Equilibrium time: 90 min	Electrostatic interactions	Sereshti et al. (2020)
Graphene nanosheets supported Lanthanum hydroxide nanoparticles	N.A.	N.A.	41.96	2.16^{L}	0.0002^{PSO}	Adsorbent dose: 0.5 g L^{-1},T = 25 °C, pH = 4, Equilibrium time: 10 h	Chemisorption process	Zhang et al. (2014)
Graphene−Lanthanum Composite	$LaNO_3$	N.A.	82.6	$N.A.^{L}$	0.1847^{PSO}	Adsorbent dose: 2 g L^{-1}, T = 25 °C, pH = 6.2, $C_{phosphate}$: 14–292 mg L^{-1}	N.A.	Chen et al. (2016)

*N.A.: Not available, L: Langmuir isotherm, F: Freundlich istotherm, PSO: Pseuodo second-order.

elements, including Zr, Fe, and La, were used in modification to optimize the phosphate removal performance. The results presented that PSO and Langmuir, respectively, commonly followed the kinetic and isotherm models. The adsorption process using GO is essential because the initial pH (2–6.2), adsorbent dose (0.2–2.0 g L^{-1}), initial phosphate concentration (5–292 mg L^{-1}), temperature (25 °C), and equilibrium time (5 min–48 h) affect the material's performance. Moreover, the surface area of the modified adsorbents and possible phosphate adsorption mechanism was also considered. The primary phosphate adsorption mechanisms were found to be electrostatic interaction and ligand exchange. The phosphate adsorption capacity of modified graphene and GO adsorbent was found in the range of 5.81–353.36 mg g^{-1}.

3.1. Unmodified graphene and GO

Vasudevan and Lakshmi (2012) developed graphene with liquid-phase exfoliation for the adsorption of phosphate. The experimental runs were conducted under different phosphate concentrations

(25–125 mg L^{-1}), temperature (303–333 K), and initial pH (2–12). Results revealed that graphene was an effective material with an adsorption capacity of 89.4 mg g^{-1} at a concentration of 100 mg L^{-1}, a temperature of 303 K, and initial pH of 7. In a separate study, GO was developed chemically to treat phosphate in aqueous solution by Jun et al. (2013). The removal efficiency was enhanced from 70 to 80% with the presence of an iron particle in chemically synthesized GO. The highest phosphate adsorption capacity was found to be 89.37 mg g^{-1} at a temperature of 30 °C, initial pH of 7, and phosphate concentration of 100 mg L^{-1}. Results showed that there was no significant difference between liquid-phase exfoliation and chemically prepared GO for phosphate removal. The GO developed by Vasudevan and Lakshmi (2012) presented similar performance compared with the Jun et al. (2013). The performance of graphene and GO in tricresyl phosphate removal at batch operation mode was also studied. The Langmuir isotherm model presented that the phosphate adsorption performance of both graphene and GO adsorbents were enhanced with increment in temperature at initial pH of 5 with the highest adsorption capacity of 30.7 mg g^{-1} for GO and 87.7 mg g^{-1} for graphene (Liu et al., 2017). Wang et al. (2019) studied reduced GO (rGO) for the potential use as an adsorbent in phosphorous removal from natural surface water and a secondary wastewater effluent containing 0.026 and 0.073 mg L^{-1}, respectively. The adsorbent with BET specific surface area of 724 m^2 g^{-1} had promising results by >90% removal efficiency from both water sources.

3.2. Modified graphene and GO

Many types of metal ions (e.g. zirconium, titanium, iron, lanthanum, and silver) have been used for the modification of GO. Zong et al. (2013) investigated the treatment of phosphate using an adsorption process with specifically synthesized zirconia-functionalized GO (Zr-GO). The prepared Zr-GO adsorbent significantly enhanced phosphate adsorption than the GO due to the strong phosphate sorption on ZrO_2 and the efficient dispersion of nano-ZrO_2 particles on the GO surface. The highest phosphate adsorption of Zr-GO adsorbent was found to be 131.6 mg g^{-1} at a temperature of 25 °C with the normalization of ZrO_2 content. Furthermore, porous zirconium-crosslinked GO/alginate aerogel beads was prepared to enhance phosphate removal and performance of adsorbent (Shan et al., 2019). The effects of initial pH (2–7), adsorbent dosage (50–500 mg L^{-1}), temperature (20–40 °C), and co-existing anions (F^-, Cl^-, NO_3^-, HCO_3^-, and SO_4^{2-}) were investigated. The optimum phosphate adsorption was achieved at low pHs in the range of 2.1–4. Consequently, the highest adsorption capacity was found to be 189.06 mg g^{-1} at an adsorbent dosage of 0.2 g L^{-1} and phosphate concentration in the range of 2–150 mg L^{-1}. This Zr-GO/Alg aerogel beads exhibited high phosphate adsorption capacity compared with Zr-GO adsorbent owing to its highly porous structure resulted with high surface area.

Moreover, the titania-functionalized GO (T-F GO) adsorbent has been studied for the removal of phosphate from synthetically prepared wastewater (Sakulpaisan et al., 2016). The adsorption capacity of titania, GO, and T-F GO adsorbents were also investigated under different contact times (30–1440 min) and initial pH (2–10) values. The adsorption performance of the specifically prepared T-F GO decreased with the increasing initial pH due to rising the repulsion between the surface charge of the T-F GO and phosphate ions. The highest phosphate adsorption capacity of 33.11 mg g^{-1} was achieved at initial pH of 6 in the presence of sodium ions compared with the titania and GO. Aragonite nanorods decorated GO (β-FeOOH/GO) is another GO-based material for recovery and removal of phosphate (Harijan and Chandra, 2017). The effects of operating variables, such as initial pH (2–12), adsorbent dose (0–0.6 g L^{-1}), and phosphate concentration (5–30 mg L^{-1}) on phosphate adsorption performance of β-FeOOH/GO adsorbent were investigated. Furthermore, different isotherm models (Langmuir and Freundlich) and kinetic models (pseudo-first-order, second-order, and solid diffusion) were determined, and the Langmuir isotherm and PSO models were well fitted better compared with Freundlich model and pseudo-first order and soil diffusion kinetics. Overall, the β-FeOOH/GO adsorbent presented the highest sorption capacity of 45.2 mg g^{-1} at initial pH of 7 and temperature of 30 °C. The adsorbent was recycled using different pH solutions (2–10), and the highest phosphate recovery of 78% was obtained at a solution pH of 10.

Among the modification agents, lanthanum is a well-known metal for the enhancement of removal performance of adsorbents. For instance, the lanthanum-modified hydroxide doped reduced magnetic GO (MG@La) composite with a high phosphate adsorption capacity was produced with lanthanum metal (Rashidi Nodeh et al., 2017). The material presented a considerably high phosphate adsorption capacity of 116. 28 mg g^{-1} at initial pH value in the range of 6–8 and equilibrium time of 30 min. Moreover, phosphate and nitrate from actual sewage and river water samples using MG@La adsorbent were carried out. The maximum removal efficiency was found to be almost 74% for phosphate and 90% for nitrate. The 3D self-assembled cellulose/graphene hybrids (3D cell/GO hybrids) is another GO-based material with the loading of lanthanum and zirconium for the phosphate adsorption from water (Polyakov et al., 2020a; Zhang et al., 2019a). The adsorption capacity was improved from 36.5 to 47.7 mg g^{-1} with the increment in pH from 2.0 to 3.0 due to the advantage in the phosphate adsorption's acidic surroundings. It was also remarkable that the adsorption of phosphate by 3D cell/GO hybrid adsorbent was temperature insensitive, and the highest removal obtained at 25, 35, and 45 °C were almost 42.5, 41.9, and 40.7 mg g^{-1}, respectively. After six cycles of adsorption/desorption, phosphate recovery was about 22.3 mg L^{-1}, accounting for about 85.8% of the initial result that indicated their stability and reusability for phosphate abatement in water.

Iron is another low-cost metal for the synthesis of GO-metal composite. The performance of nitrogen-doped reduced GO (NGO) and NGO decorated with Fe_3O_4 nanoparticles as a magnetically separable adsorbent in phosphate removal was also studied (Akram et al., 2019). The kinetic studies showed that the PSO was well fitted with the phosphate sorption by chemisorption and physisorption. Furthermore, the Freundlich isotherm model well fitted the phosphate sorption with a maximum adsorption capacity of 169.7 mg g^{-1}. Moreover, Chinnathambi and Alahmadi (2021) synthesized Fe_3O_4 anchored polyaniline intercalated GO (Fe_3O_4x%-PANI@GO) using co-precipitation and modified Hummer's method for the removal of phosphate ions and Cr (VI) (Fig. 2(a)). The magnetic properties and morphological properties of synthesized Fe_3O_4x%-PANI@GO material were determined using VSM and SEM analysis, respectively (Fig. 2(b)–(e)). The effects of operating parameters, including initial pH (3–12), co-existing anions (Cr (VI) and phosphate), and contact time (0–300 min) were investigated on the removal performance of adsorbent. The maximum phosphate adsorption capacity of 94.345 mg g^{-1} was achieved using the PSO kinetic model (k_2: 1.0184 g $(mg.min)^{-1}$). The primary removal mechanism was found as electrostatic interaction and followed by surface complexation (Fig. 2(f)).

GO modification with silver and Al_{30} polyoxocations have been less investigated compared with above-mentioned metals. For instance, Vicente-Martínez et al. (2020) conducted a comparative study on GO and GO functionalized with silver nanoparticles (GO@AgNPs) for phosphate removal from an aqueous solution with an adsorption process. The experimental conditions, including initial pH (1–14), initial phosphate concentration (10–30 mg L^{-1}), reaction time (0–20 min), adsorbent dose (GO: 10–50 mg, GO@AgNPs: 100–500 μL), and temperature (293–333 K) were studied to achieve the highest adsorption capacity. The maximum phosphate removal efficiency of 100% was achieved using a relatively high amount of GO compared with GO@AgNPs adsorbent. The maximum phosphate adsorption efficiency was found to be 75% using GO at a reaction time of 9 min, adsorbent dose of 20 mg, initial pH 10, temperature of 293 K, and initial phosphate concentration of 30 mg L^{-1} achieving the highest adsorption capacity of

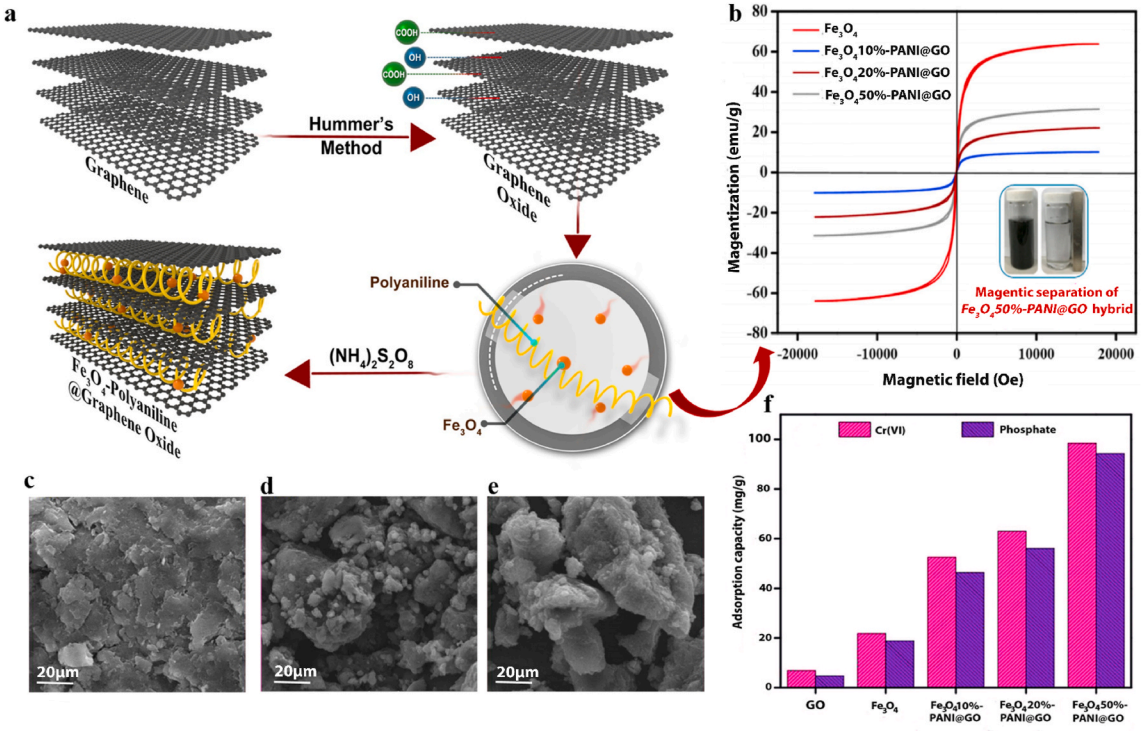

Fig. 2. (a) Preparation of Fe_3O_4x%-PANI@GO adsorbent, **(b)** VSM analysis of Fe_3O_4, $Fe_3O_4$10%-PANI@GO, $Fe_3O_4$20%-PANI@GO, and $Fe_3O_4$50%-PANI@GO, **(c)** SEM of GO, **(d** SEM of Fe_3O_4, **(e)** SEM of $Fe_3O_4$50%-PANI@GO, and **(f)** Phosphate adsorption capacity of the synthesized adsorbents (initial phosphate concentration: 100 mg L^{-1}, adsorbent dose: 100 mg, operating time: 300 min, and mixing speed: 200 rpm). Adapted from [Chinnathambi and Alahmadi, 2021] with permission from Elsevier (License number: 5070320778125).

11.25 mg g^{-1}. On the other hand, the highest phosphate removal efficiency of 100% was achieved using GO@AgNPs at similar operating conditions except for an adsorbent dose of 500 μL and initial pH of 7, achieving a maximum adsorption capacity of 1666.7 mg g^{-1}. Furthermore, the regeneration of adsorbents was determined using the acid medium. The regeneration percentages were 80% for GO@AgNPs and 98% for GO, which indicated that the adsorbents' satisfactory regeneration performance allows them to be reused and recycled. The oxyanion (phosphate, chromate, and selenate) adsorption performance of Al_{30} polyoxocations-modified GO nanosheets was also studied (Tahmasebi, 2020). Furthermore, the FTIR and TGA analysis showed that phosphate anion's primary adsorption mechanism was inner-sphere surface complex formation with Al_{30} surfaces. The Langmuir monolayer isotherm model achieved the maximum phosphate adsorption capacity of 185.2 mg g^{-1}. The phosphate adsorption capacities and adsorbent dosages of ferrihydrite loaded on the GO (FeOOH-GO), zirconium-loaded reduced GO (Zr-rGO), graphene-lanthanum composite (La-Graphene), GO decorated with α-Fe_2O_3 (α-Fe_2O_3-GO), lanthanum functuonlized GO (La-GO), zirconium functionalized nanochitosan-GO (Zr–NCH-GO), graphene aerogel, and triethylene tetramine functionalized magnetic GO chitosan composite (TT-Fe–CH–GO) materials were presented in Fig. SM3. The highest phosphate adsorption capacities of 353.4 and 350 mg g^{-1} were achived using TT-Fe–CH–GO and graphene aerogel materials owing to high surface area and phosphate adsorption affinity, respectively. On the other hand, the minimum adsorption capacity of 5.81 mg g^{-1} was observed using FeOOH-GO composite at adsorbent dosage of 1.33 g L^{-1}.

There are also some other interesting applications of GO as hybrid material recently published in the literature. A facile and cost-effective strategy was followed to prepare a cobalt and nitrogen codoped three-dimensional (3D) graphene catalyst by inserting carbon nanospheres into the interlayers of graphene sheets for both the oxygen reduction and oxygen evolution reactions (ORR/OER) in rechargeable metal–air batteries and unitized regenerative fuel cells (Qiao et al., 2016). A composite material that consists of graphene oxide (GO) sheets were crosslinked with N-hydroxysuccinimide (NHS) and functionalized with gold nanoflowers (AuNFs) for sensitive detection of chloramphenicol antibiotic (Ali et al., 2021).

4. Lignin

Lignin, one of the most abundant renewable materials, is significantly composed of polymer (B. Wang et al., 2017). A significant amount of lignin waste is commonly used for energy production, while relatively low amount of it used as a value-added material and chemical (Liu et al., 2016a, 2016b, 2016b). However, the lignin has promising potential as an adsorbent owing to its ease of biodegradability and high functional groups. Up to date, several studies conducted on removal of heavy metals and dyes from aqueous solutions using lignin based adsorbents (Thakur et al., 2017). The use of raw lignin to remove phosphate was found to be inefficient due to electrostatic repulsion between negatively charged phosphate and negatively charged functional groups, such as $COOH^-$, and OH^- on lignin surface. Therefore, lignin has been modified to increase the phosphate removal performance. Nevertheless, there are limited studies on phosphate removal from aqueous solutions using modified lignin-based materials.

Zong et al. (2016) prepared zirconia-loaded lignocellulosic butanol residue (LBR-Zr) as a biosorbent for the adsorption of phosphate an aqueous solution. The highest phosphate adsorption capacity of LBR-Zr was found to be 8.75 mg g^{-1}. The thermodynamic experiments presented that the phosphate adsorption performance of adsorbent improved with the increase in temperature from 298 to 338 K. Moreover, Zhao et al. (2020) prepared interfacial diethylenetriamine-modified aminated lignin integrated with zirconium hydroxide (AL-DETA@Zr) adsorbent for phosphate recovery. Maximum phosphate adsorption capacity was found to be 167.7 mg g^{-1}.

Furthermore, the kinetic data was well fitted with PSO kinetic model (R^2: 0.992 and rate constant: 0.005 g (mg.min)$^{-1}$) and showed that the adsorption process was chemisorption.

Magnetic lignin-based materials have been studied for phosphate removal due to the easy separation of adsorbents after the removal process with application of magnet. In this regard, the iron-complexed lignin was synthesized for treatment of low phosphate-containing water. The lignin was obtained by liquor from the paper industry and modified using triethylenetetramine through the Mannich reaction, and then lignin was chelated with $FeCl_3$ salt to make the iron-complexed lignin as an environmentally friendly and cost-effective lignin-based adsorbent. The kinetic and isotherm models were followed by PSO and Langmuir model, which shows monolayer adsorption. The basis of the Langmuir equation, the values of Q_{max} were 0.924, 0.912 and 0.942 mg g^{-1} for adsorbent at temperature of 298, 308 and 318 K, respectively. Main phosphate adsorption mechanism of iron-complexed lignin was found as complexation between phosphate and iron on the adsorbent surface. At initial phosphate concentration of 5 mg L^{-1} and adsorbent dose of 1 g, the maximum removal efficiency of iron-complexed lignin was found to be >90%. In addition, the reusability of the adsorbent was determined with cycle adsorption experiments and results revealed that the phosphate removal efficiency of adsorbent decreased from 95.3 to 82.3% at the end of the second cycle, most probably after the regeneration process, the active sites of the adsorbent was relatively irreversible due to the strong bonding between phosphate and adsorbent (Luo et al., 2017). Li et al. (2021) also synthesized magnetic aminated lignin based adsorbent (M/ALFe) for separation and recovery of phosphate in water and then reprocessed as a renewable magnetic fertilizer (Fig. 3(a)). The magnetic properties of the aminated lignin and M/ALFe were determined and results showed that the synthesized adsorbent presented highly sensitive magnetic feature and can be separated using magnet from soil, while the aminated lignin did not show magnetic property (Fig. 3(b)). Moreover, the effects of adsorbent dose (0.1–0.8 g L^{-1}) and initial pH (3–9) on phosphate removal performance of adsorbent were studied. The phosphate adsorption capacity of adsorbent decreased with increasing adsorbent dose most probably due to the decrease of phosphate concentration with M/ALFe dose. On the other hand, the phosphate removal efficiency increased from 17.95 to 85.17% with the increase in adsorbent dose from 0.05 to 0.7 g owing to increasing available adsorption sites. Both phosphate removal efficiency and adsorption capacity increased significantly from initial pH 3 to 9, while the performance of adsorbent was decreased at pH 11 due to the dissolution of aminated lignin in solution. Finally, the optimized adsorbent was tested as a fertilizer and results obviously showed that after the use in soil, the adsorbent could be easily recovered from soil using magnet (Fig. 3(c)).

Lanthanum has also been used for lignin modification to enhance phosphate removal. For instance, Zong et al. (2018) recommended poly (ethyleneimine)-graft-alkali lignin loaded with nanoscale lanthanum hydroxide (AL–PEI–La) for effective phosphate removal. The phosphate removal efficiency of 94% was achieved at initial phosphate concentration of 50 mg L^{-1} in 60 min. In comparison, the removal efficiency of 99% was observed at low phosphate concentration of 2 mg L^{-1} in 15 min and the phosphate concentration considerably reduced to limit value of <50 μg L^{-1} for the prevention of eutrophication. The highest phosphate adsorption capacity of AL–PEI–La adsorbent was found to be 65.79 mg g^{-1} that 33 times higher than lignin adsorption capacity. The main adsorption mechanism of AL–PEI–La adsorbent was most probably an interaction between ligand exchange and surface precipitation. Furthermore, the recyclability of the adsorbent was determined with desorption experiments and results showed that 85.8% of the adsorption capacity remained after 3 cycles. The phosphate removal using lignin-derived porous carbon loaded with $La(OH)_3$ nanorods (LPC@La $(OH)_3$) was studied by Liu et al. (2019a, 2019b, 2019c). The synthesized LPC@$La(OH)_3$ adsorbent presented a significant phosphate adsorption capacity of 60.24 mg g^{-1} at La content of 28.72%, temperature of 25 °C, initial phosphate concentration in the range of 36.5–105 mg L^{-1}, initial pH in the range of 3–10. Adsorption experiments showed that at the

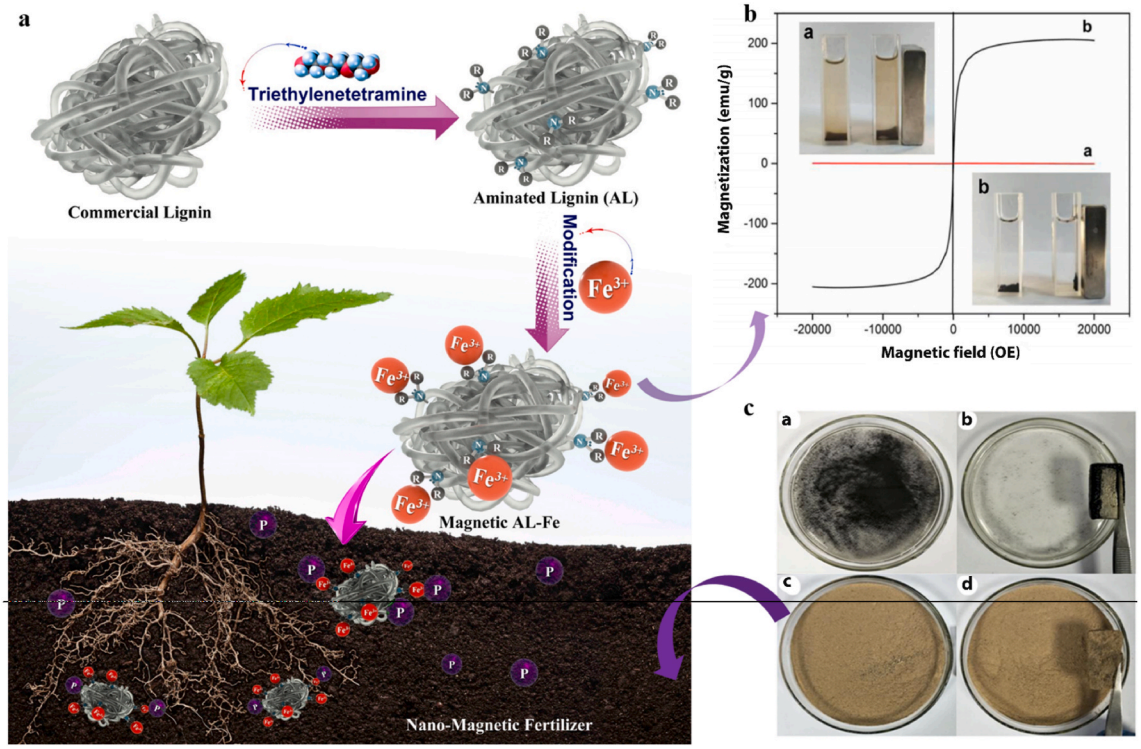

Fig. 3. (a) Schematic diagram of preparation and application of magnetic aminated lignin based (M/ALFe) adsorbent, **(b)** VSM analysis of aminated lignin (a) and M/ALFe (b) adsorbent, and **(c)** M/ALFe adsorbent before (a) and after (b) magnetic separation and M/ALFe adsorbent-soil mixture before (c) and after (d) magnetic separation. Adapted from [T. Li et al., 2021] with permission from Elsevier (License number: 5070321255573).

initial phosphate concentration of 2 mg L^{-1}, the ultrafast phosphate adsorption capacity of 99.5% was achieved in a reaction time of 10 min. Furthermore, the recyclability of adsorbents was tested to understand the practical application on a real scale. The phosphate removal efficiencies of LPC@$La(OH)_3$ were found to be 100, 93.5, and 92.7% at the end of the first, second, and third regeneration test, respectively. The adsorbent provided sufficient regeneration performance as presented by a significant phosphate removal efficiency still >90% after three-cycle. To understand the adsorption mechanism of developed LPC@$La(OH)_3$ adsorbent, the specified amount of adsorbent was added into the KH_2PO_4 solution and the pH change in the solution was measured. The pH of the solution increased from 5.76 to 7.46 in 24 h most probably due to the leaching out of hydroxide ions by ligand exchange. Overall, both ligand exchange and chemical precipitation were found as the main adsorption mechanism of LPC@$La(OH)_3$ adsorbent for phosphate removal (Xiaohuan Liu et al., 2019a, 2019b, 2019c). Liu et al. (2020) developed cerium oxide nanoparticle (nano-CeO_2) functionalized lignin (L-NH_2@Ce) as a nano-biosorbent by a facile *in-situ* precipitation method for selective phosphate removal. The surface area of lignin and L-NH_2@Ce adsorbents was analyzed using BET technology and the L-NH_2@Ce surface area was found to be 89.8 m^2 g^{-1}, which is 3 times higher than the lignin. Therefore, the phosphate adsorption capacity of L-NH_2@Ce improved from 1.92 to 27.86 mg g^{-1} compared with lignin. The results revealed that the L-NH_2@Ce nano-biosorbent could rapidly decrease a high phosphate concentration of 10 to below the 0.5 mg L^{-1} of discharge standard for drinking water according to the World Health Organization (WHO).

Modification of lignin with magnesium oxide was reported by Jiao et al. (2021). The authors fabricated MgO-functionalized lignin-based bio-charcoal (MFCL) for phosphate removal from water. The MFCL adsorbent showed significant regeneration feature for phosphate adsorption owing to the suitable morphology of MgO nanoparticles and it may also be used in a pH range of 2–10. Furthermore, the high amount of MgO nanoparticles loading has considerably enhanced the activity of MFCL. For instance, the MFCL phosphate adsorption capacity was increased from 145.25 to 258.63 mg g^{-1} with the increasing MgO nanoparticles content percentage from 14.18 to 28.41%. The highest phosphate capacity of MFCL was found to be 906.8 mg g^{-1}. Adsorption-desorption experiments provided that the main phosphate adsorption mechanisms of adsorbents were ligand exchange and single layer chemisorption.

The hydrated metal hydroxides, such as zirconium oxide, iron salts, lanthanum oxide, cerium oxide, and magnesium oxide, have been immobilized onto lignin waste to enhance the phosphate adsorption performance and surface area. Among these metal hydroxides, lanthanum oxide is gained particular interest owing to its significant stability, low toxicity, high removal performance and adsorption capacity, and usability at a wide range of pHs. The phosphate adsorption mechanism may include hydrogen bonding, precipitation, ligand exchange, crystallization, inner and other complexation, and electrostatic interaction. In most of the above-mentioned studies, the main adsorption mechanism was reported as electrostatic interaction, chemical precipitation, and ligand exchange, while PSO and Langmuir model, respectively followed the kinetic and isotherm models. The phosphate adsorption capacities of modified lignin-based materials were found to be in the range of 8.75–906.8 mg g^{-1}.

5. Carbon nanotubes (CNTs)

CNTs, including single and multi-wall (SWCNTs and MWCNTs), are relatively materials used for phosphate removal with the adsorption process. The features of CNTs, such as high surface area, significant mechanical strength, nano-scale sizes, stability, and flexibility, make them a promising material for the adsorption of pollutants like phosphate from aqueous solutions (Huang et al., 2018). Several studies were conducted on removing copper, lead, herbicides, antibiotics, nitrogen, and cyanobacterial toxins using CNTs (Zaytseva and Neumann, 2016). However, the use of CNTs to remove phosphate has been investigated in a few research up to date. Commonly, the CNTs have been modified with La, Zr, and chitosan to enhance the phosphate adsorption capacity. For instance, Mahdavi and Akhzari (2016) studied CNTs for their phosphate removal potential. The experimental data were well fitted with the Freundlich model, and adsorption capacity was found 15.4 mg g^{-1}.

A carboxylated MWCNTs adsorbent loaded with lanthanum hydroxide (MWCNTs–COOH–La) was prepared and studied to treat phosphate in batch operation mode. The highest adsorption capacity was found to be 48.02 mg g^{-1}. The phosphate adsorption behaviors were defined by the PSO, indicating that the adsorption behaviors were predominantly approved to chemisorption (Zong et al., 2017). Huang et al. (2018) designed a sustainable adsorbent for phosphate removal by modifying MWCNT with chitosan through simply cross-linking. They found a maximum adsorption capacity of almost 36.1 mg g^{-1} achieved at 293 K and pH 3 in 30 min. Furthermore, the developed adsorbent's adsorption capacity could be sustained at 94–98% even after five adsorption-desorption cycles. An effective zirconium-modified CNTs (Zr-CNTs) adsorbent was developed to treat phosphate in solution with batch mode. The adsorption quantity was determined to be 10.9 mg g^{-1} at 303 K. The kinetic data were better correlated with the Elovich model, suggesting that the adsorption process may be chemisorption (Gu et al., 2019). Wang et al. (2019) also prepared CNT in the same study mentioned in the GO part for the phosphorus recovery (Fig. 4(a)). The adsorbent having 242 m^2 g^{-1} of BET surface area showed many performances and around 95% removal percentage from both surface water and wastewater effluent (Fig. 4(b)). The experimental fitted into the Freundlich model, suggesting heterogeneous surface adsorption behavior. Furthermore, the XPS analysis was conducted to understand the primary adsorption mechanism of CNT with C1s spectrums. As presented in Fig. 4(c)–(d), the spectrums showed that the C–OH, C═O, and COOH oxygenated functional groups on the surface of the CNT increased at the end of both surfaces and wastewater adsorption experiments. The metals, such as lanthanum and zirconium, have been loaded onto MCNT to enhance the phosphate adsorption performance and affinity of adsorbent. Among these metals, lanthanum immobilization on MWCNTs is gained significant interest due to its high phosphate adsorption capacity. The effects of conatact time, pH, and temperature have been investigated to optimize MWCNT phosphate removal performance. Moreover, the main phosphate adsorption mechanism was reported to be chemisorption. The adsorption capacities of modified CNT and MWCNTs were found to be in the range of 10.9–48.02 mg g^{-1}.

6. gC_3N_4 and other carbonaceous materials

The gC_3N_4 has attracted the attention of scientist due to its potential application in photosynthesis, adsorption, and electrocatalysis. Moreover, it can be used to support stable metal and metal oxide to synthesized porous structure adsorbent. Recent years a large number of materials, including metals, metal oxides, and carbonaceous materials have been combined with gC_3N_4 to improve adsorption performance (Gamshadzehi et al., 2019). For example, Wan et al. (2019) developed protonated graphite carbon nitride and acid-activated montmorillonite (g-C_3N_4/Mt) composite and evaluated its performance for phosphate removal efficiency from an aqueous medium. While the saturated adsorption capacity of bare g-C_3N_4 with 5.98 m^2 g^{-1} of BET surface area was only 1.56 mg g^{-1}, the removal efficiency of the as-prepared composite (2.0%-g-C_3N_4/Mt) with 128.72 m^2 g^{-1} of BET surface area was remarkably elevated due to the synergistic effects and the saturated adsorption capacities of phosphate was found to be 5.06 mg g^{-1}. The isoelectric point of protonated g-C_3N_4 was determined as pH of 5.2. A microporous Fe_2O_3 loaded porous carbon nitride (Fe_2O_3/g-C_3N_4) adsorbent was prepared via a one-pot synthesis route for the removal of phosphate from synthetic water. The removal efficiency was higher than 90% for high ionic strength, adsorbent dose of 1g L^{-1}, and broad pH

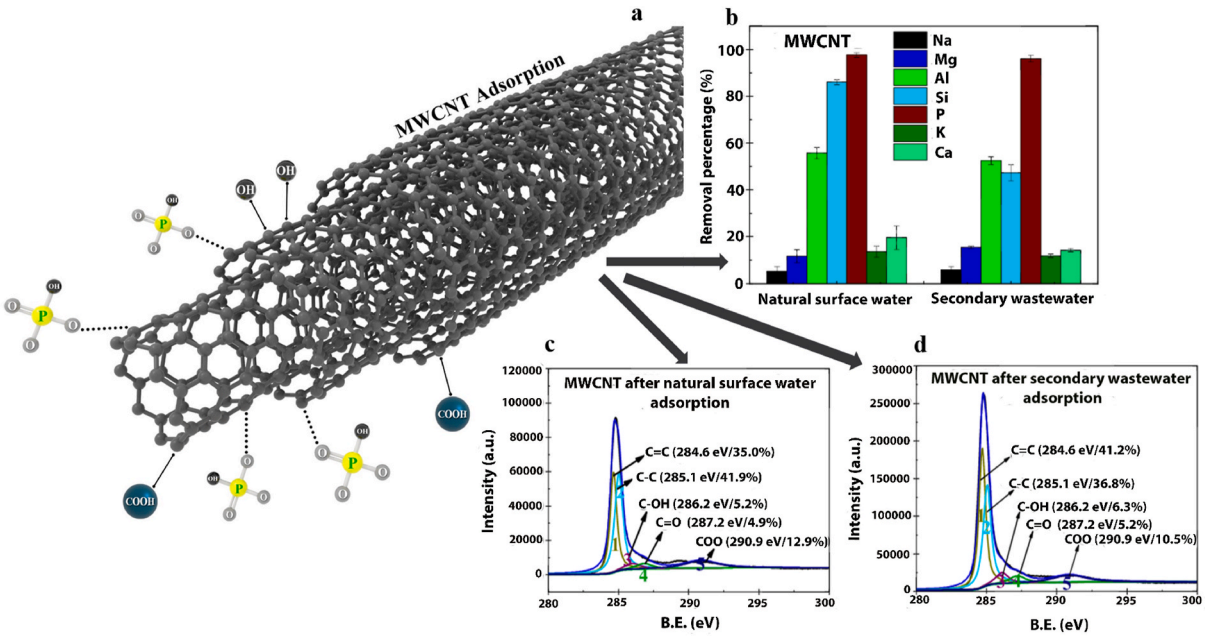

Fig. 4. (a) Schematic diagram of the adsorption mechanism of HPO_4 species with multi-wall carbon nanotube (MWCNT); **(b)** Removal performance of MWCNT for ions in surface and wastewater; **(c)** XPS C1s spectrum of MWCNT after the treatment of natural surface water; and **(d)** XPS C1s spectrum of MWCNT after the treatment of secondary wastewater. Adapted from [Yifei Wang et al., 2019] with permission from Elsevier (License number: 5070330152172).

range (3–10) with a relatively short equilibrium time of 15 min. The sorption capacity was 17.11 mg g^{-1} that was higher than that of most of the adsorbents except those containing La compounds (Gamshadzehi et al., 2019).

Moreover, Almanassra et al. (2020) used carbide-derived carbon (CDC) for phosphate removal from treated sewage effluent. The titanium carbide (TiC) powder was utilized as a precursor for CDC synthesis. In the batch adsorption experiments, the CDC showed an adsorption capacity of phosphate of 16.14 mg g^{-1} whose adsorption efficiency was not affected by the temperature. In a separate study, Koilraj and Sasaki (2017) designed a composite material of porous carbon (PC) produced from sucrose with the reported modification and lanthanum to selective phosphate from aqueous solutions. La-PC composite possessed 40.74 mg g^{-1} of Langmuir adsorption capacity. MgO-doped ordered meso-porous carbon (OMC-MgO) was synthesized by evaporation-induced self-assembly (EISA) in one-pot with biomass-derived gallic acid instead of phenolics as carbon precursor, metal ion Mg^{2+} instead of formaldehyde as cross-linking agent and F127 as template. As-prepared at 800 °C, a perfectly-ordered meso-porous structure centered at (6–8) nm, OMC-MgO-T800 had a specific surface area of 808 m^2 g^{-1}, and showed good performance for phosphorus removal from aqueous solutions with a maximum sorption capacity of 107 mg g^{-1} (Liu et al., 2021). Moreover, black liquor-derived calcium-activated biochars (Ca-biochar) were synthesized by treating rice straw with $Ca(OH)_2$ to create an adsorbent that was effective for removing phosphate from aqueous waste streams. The Ca-biochar adsorbent was efficient for the removal of phosphate from aqueous solutions (pH 1.0 to pH 13.0) with a highest phosphate adsorption capacity of 197 mg g^{-1} (Xiaoning Liu et al., 2019a, 2019b, 2019c). However, Almanassra et al. (2021) reviewed various kinds of biochars to remove and recover phosphate from aqueous solutions including adsorption mechanism, isotherm, kinetics, thermodynamics, and capacities by comparison. Therefore, we have not included biochar as one of the carbonaceous materials in this review.

On the other hand, there are some other applications of carbon nanotubes as hybrid materials developed for pesticide detection, such as single-walled carbon nanotube (SWCNT) as three-dimensional porous hybrid material (SWCNT-Pc 3D) and its copper complex (Cu-SWCNT-Pc 3D) (Şenocak et al., 2021), SWCNT functionalized by ZnPc containing three boron dipyrromethene (BODIPY) (Köksoy et al., 2021a) and one ethyloxy azido moieties and a hybrid carbon nano-material (SWCNT-SubPc-Pc) bearing subphthalocyanine substituted zinc (II) phthalocyanine conjugate on the SWCNT (Köksoy et al., 2021b). Air-stable cobalt decorated-nanoporous carbon (Co/ZIF-C), derived from the pyrolysis of zeolitic imida-zolate based metal-organic framework (ZIF-67), for ultrasensitive detection offlavonoid, rutin is another sensor application of CNTs (Şenocak et al., 2020). Single walled carbon nanotubes (SWCNT) with 3-phenylcoumarin derivatives on the chemiresistive sensor response to ammonia were synthesized by different types of functionalization (M. S. Polyakov et al., 2020). M. Polyakov et al. (2020) was also studied the novel hybrid nanomaterial SWCNT/SiPc made of single walled carbon nanotubes (SWCNT) cross-linked via axially substituted silicon (IV) phthalocyanine (SiPc) as the active layer of chemiresistive layers for the detection of ammonia and hydrogen.

7. Recovery of phosphate from carbonaceous materials

Along with nitrogen and potassium, phosphorus is essential for plant life, which helps in root development, plant maturation, and seed development. Unfortunately, the soil gets depleted of phosphorus due to several reasons, including being washed away by rain (Bradford-Hartke et al., 2021). Therefore, modern farming is reliant on the use of phosphorus-based fertilizers significantly. By meeting approximately two-thirds of the world's phosphate resources, sedimentary and marine phosphate rock deposits are used to manufacture commercial phosphate fertilizers. Ground rock phosphate has been used as a source of phosphorous for soils in the past. However, due to the low concentration of phosphorous in this native material, high transportation costs, and small crop responses, rock phosphate usage has reduced considerably in agriculture (Günther et al., 2018). In addition to the direct use of manure and digestates, solubilized phosphorus speceis recovery has become desirable in wastewater treatment plants nowadays. Several technologies have been conducted to phosphorous recovery from aqueous solutions, including biological removal (Seviour et al., 2003), crystallization (Xuechu et al., 2009), adsorption (Vera-Puerto et al., 2020), and precipitation (Zhang et al., 2013). On the other hand, the chemical addition

and source of aqueous solutions significantly affect phosphorus speceis recovery's applicability. For instance, the high energy consumption, high cost, and high heavy metal contents are the main drawbacks of phosphorus speceis recovery from wastewater sources. The sorption of aqueous phosphorus in fixed-bed and suspension-based systems is an alternative method in which the materials employed for phosphorous adsorption are either used directly as fertilizers or regenerated for phosphorus recovery reused (Mayer et al., 2016). These materials' desorption capability is of utmost importance since phosphate is considered a ''non-renewable resource,'' and it may be depleted in less than a century due to the world growing demands. This principle is valid for all previously mentioned carbonaceous materials in this review. After each adsorption process, the phosphate ions were desorbed from the saturated sorbents using various eluents such as ethanol, HCl, NaCl, and NaOH at different concentrations. Then, the adsorbent was washed with excess distilled water to the appropriate pH (Sowmya and Meenakshi, 2013).

The phosphorus speceis recovery process from graphene and GO materials widely conducted using NaOH solution. For instance, the phosphate removal from water using GO-Fe_2O_3 material was studied under optimum operating conditions (initial phosphate concentration: 50 mg L^{-1}, pH: 6, adsorbent dose: 32.5 mg, and reaction time: 2 h), and then regeneration experiments were conducted to understand the recovery potential of adsorbent. The maximum phosphate desorption efficiency of 79% was achieved using NaOH solution (pH: 14) at a reaction time of 2 h (Bai et al., 2018). H. Wang et al. (2017) conducted phosphate desorption experiments from triethylene tetramine-modified magnetic GO (TETE-MGO) using 1 M NaCl and 1 M NaOH mixture, and the optimum phosphate desorption was found to be >80% for every three cycles. In a separate study, the phosphate recovery from Zr/La-cell/GO was performed using 0.5 or 5 wt% of NaOH solutions under the operating time of 60 min. The phosphate recovery was found as almost 85% using 5 wt% of NaOH solution after six cycles (L. Zhang et al., 2019). The phosphate exhausted GOAZr adsorbent was regenerated with 0.1 M NaOH solution and reused in 11 cycles. The maximum recovery efficiency was 95%, which showed that the GOAZr adsorbent is significantly stable and reusable (Zong et al., 2013). Salehi and Hosseinifard (2020) conducted recovery of phosphate from exhausted zirconium loaded nano chitosan GO (NCS@GO) adsorbent. The recovery efficiency was found to be >76%. No significant change was observed for phosphate recovery in 10 cycles. On the other hand, literature studies with lignin-based materials extensively focused on the regeneration of materials by NaOH and HCl solutions after the phosphate removal process rather than phosphate recovery potential. Zong et al. (2018) obtained that the adsorption capacity of 98.4% (66.94 mgP g^{-1}) for AL-PEI-La material was remained constant at the end of the first cycle, which means that the after regeneration process 65.84 mg g^{-1} phosphate recovered from the adsorbent. In another study, the regeneration of L-NH2@Ce was provided using 0.1 NaOH solution at a temperature of 60 °C with two cycles to recover the phosphate from the exhausted adsorbent. The phosphate removal efficiency of the material decreased from 92 to 90% at the end of the second cycle, most probably due to the slight decrease of active surfaces of material after regeneration tests (Liu et al., 2018). Zhao et al. (2020) also reported the regeneration of phosphate contaminated AL-DETA@Zr material by NaOH solution at different cycles. After the three cycles, the phosphate adsorption performance of the material was remained constant at the capacity of 88.6 mg g^{-1}. Furthermore, the regeneration of phosphate exhausted lignin-based material using HCl solution has been reported (Li et al., 2021). After the phosphate removal process, the M/ALFe material was fed in the HCl solution and then collected by a magnet. The recovery efficiency of the adsorbent was found as 83.0% at the end of the six cycles. The slight decrease in recovery efficiency was most probably due to iron particles' leach and the degradation of lignin.

The phosphate exhausted ZrCNTs were treated with H_2O, HCl, and NaOH solutions. Among these solutions, 0.1 M NaOH has presented the highest regeneration and desorption performance with the efficiency of 86.8 and 53.5% at the end of the three cycles, respectively, owing to the ion exchange process between the phosphate and hydroxide ions on the surface of the material (Gu et al., 2019). Huang et al. (2018) also studied the reusability of chitosan/MWCNTs material with five desorption cycles. The XPS analysis provided that the phosphate percentage on the material's surface was 3% after the adsorption. In comparison, its percentage was found to be 0% at the end of the desorption process. Overall, the phosphate was entirely recovered from the material's surface and chitosan/MWCNTs material. Similarly, there is another study about the phosphate recovery from gC_3N_4 adsorbent using NaOH solution. The recovery percentage of phosphate from gC_3N_4 was found to be 83%, and the results provided that gC_3N_4 could be helpful in reutilizing and phosphate preconcentration principles (Gamshadzehi et al., 2019). Consequently, the phosphate removal and recovery potentials of carbonaceous materials make them promising, cost-effective, and eco-friendly considering the green treatment process approach. Moreover, the phosphate from water and wastewater sources could be recover and used as a phosphate source in areas with insufficient phosphorus ores.

8. Limitations of carbonaceous materials

Although adsorbents used in this review are eco-friendly due to being carbonaceous materials-derived, phosphate elution required unique, expensive, and non-green techniques. Carbonaceous materials progressively deteriorated in the capacity as the number of cycles increased, and spent adsorbents may be considered hazardous waste after that point and must be eliminated properly. Relatively high capital and operating costs could be needed for the industrial scale-up, which contains sophisticated pumps and columns and possible prefiltering operation for the feed stream to remove any particles capable of plugging adsorbent. Since phosphate adsorption is mostly endothermic, heating of the system may be needed to enhance the phosphate removal efficiency. Also, due to phosphate ions' chemical nature depending on its dissociation in aqueous solution concerning pH, as low as pH of 4 is required to obtain high removal efficiency that results in high acid consumption. Unmodified carbonaceous adsorbents' surfaces are predominantly net negatively charged, which confers them only little ability to absorb anionic pollutants. To improve the phosphate adsorption performance of them, cation-modified carbonaceous adsorbents should be developed. However, these cation-modification methods' feasibility is strongly controlled by the cost of the metal salts and their environmental friendliness. Besides, La modified adsorbents have relatively lower adsorption capacity because bulk lanthanum nanoparticles turned to aggregate in water, which led to incomplete accessibility of La to coordinate with and resulted in low La utilization efficiency. Meanwhile, using those materials in fine form in continuous chromatographic separation is difficult to apply from practical applications due to the trouble in recovery-related problems.

9. Conclusions and future perspectives

In this review, the studies about the adsorptive phosphate removal and recovery in aqueous solutions using carbonaceous materials including unmodified and modified AC, graphene, GO, lignin, CNTs, gC_3N_4, and others have been discussed and summarized. The adsorbents' synthesis methods, optimum operating conditions, surface features of the adsorbents, adsorption capacities and removal efficiencies, and adsorption mechanisms were discussed. Moreover, the kinetics, isotherms, thermodynamics, reusability of adsorbents, and possible advantages of carbonaceous materials on phosphate removal applications from water sources were also explained. The primary phosphate adsorption mechanisms were ligand exchange, precipitation, and electrostatic attraction for most synthesized carbonaceous materials. The reviewed studies' kinetic models were followed by a PSO kinetic model,

which indicates that the phosphate removal from a solution is due to a chemical reaction between phosphate and adsorbent surface.

The phosphate adsorption capacity of unmodified carbonaceous materials mainly depends on the adsorbent's surface features and mineral composition. For instance, the unmodified AC adsorbents that indicate Ca, Mg, and Zn ions within their structure have presented the highest phosphate adsorption capacity of 102 mg g^{-1} among the unmodified AC adsorbents. Regarding modified ACs, the ACs loaded with Fe ions were presented significant enhancement in AC's phosphate adsorption performance. Besides Fe ions, Ag, Al, Ca, Zr, Zn, and La were also used to impregnate the ACs to increase phosphate adsorption capacity. The maximum phosphate adsorption capacity of modified AC was found to be 151.1 mg g^{-1} for cork powder- AC stabilized nano-zerovalent iron (AC/nZVI). Similarly, the phosphate adsorption capacity of the graphene and GO materials was significantly enhanced with the modification of adsorbent. The highest adsorption capacity was 189.07 mg g^{-1} for porous Zr-crosslinked GO-alginate aerogel beads, while the maximum adsorption capacity was unmodified graphene was 89.4 mg g^{-1}. Furthermore, among the modified lignin-based adsorbents, the maximum phosphate adsorption capacity of 906.8 mg g^{-1} was achieved by functionalizing the lignin-based bio-charcoal with MgO. On the other hand, the modified CNTs and gC_3N_4 materials were presented relatively low phosphate adsorption capacities compared with other carbonaceous materials. Among these carbonaceous materials, the AC-based materials are more advantageous in terms of cost since these materials are manufactured from several waste materials such as plastics, agricultural by-products, coal, rice husk, coconut shell, and banana waste.

Most carbonaceous materials presented promising phosphate removal performance from waters as environmentally friendly, cost-effective, readily biodegradable, and nontoxic adsorbents. However, there are still gaps in the literature, which are needed to be overcome to enhance the performance of carbonaceous adsorbents for phosphate removal. For instance, the Al, Fe, La, and Zr elements were widely used for carbonaceous adsorbent modification with different sources. However, there is insufficient research on the carbonaceous materials from the same sources loaded with the same elements to compare their phosphate adsorption performance. Furthermore, recovery of phosphate from carbonaceous materials, the reusability of materials, and leaching of the loaded elements for modification should be investigated in more detail to enhance adsorbents' applicability on a real scale. To our best knowledge, there is little research on phosphate removal from aqueous solutions in the presence of other ions using carbonaceous adsorbents. However, the adsorption experiments should be conducted by mimicking real wastewater sources to understand the combined effects of phosphate and other ions on adsorbents' removal performance. The most critical gap in the literature is that the studies have been conducted at a lab scale. Therefore, further pilot and real-scale applications should be performed. Moreover, the leaching of metals incorporated with carbonaceous material may cause environmental problems in soil and water media. Therefore, the fixation of metallic groups in the carbonaceous material can be a novel interest of research to prevent such hazards to the environment. Overall, the environmental impacts, cost assessment, and ecological and human health risks of the synthesized adsorbents should be considered in future studies to achieve a realistic perspective on applicability on an industrial scale.

Declaration of competing interest

The authors declare that they have no known competing financial interests or personal relationships that could have appeared to influence the work reported in this paper.

Acknowledgments

Y. Orooji acknowledges the financial support provided by Nanjing Forestry University (Grant Nos. NFU163020203, NFU163020217 and NFU163020816) and National Natural Science Foundation of China (5201101466).

Appendix A. Supplementary data

Supplementary data to this article can be found online at https://doi.org/10.1016/j.chemosphere.2021.132177.

Credit author statement

Yasar Kemal Recepoglu: Writing-Original draft preparation, Investigation; **Aysegul Yagmur Goren**: Writing-Original draft preparation, Investigation; **Yasin Orooji**: Visualization, Reviewing and Editing; **Alireza Khataee**: Supervision, Reviewing and Editing.

References

Akram, M.Y., Ahmed, S., Li, L., Akhtar, N., Ali, S., Muhyodin, G., Zhu, X.Q., Nie, J., 2019. N-doped reduced graphene oxide decorated with Fe3O4 composite: stable and magnetically separable adsorbent solution for high performance phosphate removal. J. Environ. Chem. Eng. 7 (3), 103137. https://doi.org/10.1016/j.jece.2019.103137.

Al-Zboon, K.K., 2018. Phosphate removal by activated carbon–silica nanoparticles composite, kaolin, and olive cake. Environ. Dev. Sustain. 20, 2707–2724.

Ali, M.R., Bacchu, M.S., Al-Mamun, M.R., Ahommed, M.S., Aly, M.A.S., Khan, M.Z.H., 2021. N-Hydroxysuccinimide crosslinked graphene oxide–gold nanoflower modified SPE electrode for sensitive detection of chloramphenicol antibiotic. RSC Adv. 11, 15565–15572.

Almanassra, I.W., Kochkodan, V., Subeh, M., Mckay, G., Atieh, M., Al-Ansari, T., 2020. Phosphate removal from synthetic and treated sewage effluent by carbide derive carbon. J. Water Process Eng. 36, 101323.

Almanassra, I.W., Mckay, G., Kochkodan, V., Ali Atieh, M., Al-Ansari, T., 2021. A state of the art review on phosphate removal from water by biochars. Chem. Eng. J. 409, 128211. https://doi.org/10.1016/j.cej.2020.128211.

Astuti, W., Zulaechah, L.S., Kristian, L., 2019. Teak leaf-based activated carbon for phosphate removal. J. Bahan Alam Terbarukan 8, 52–58.

Bai, L., Yuan, L., Ji, Y., Yan, H., 2018. Effective removal of phosphate from aqueous by graphene oxide decorated with α- Fe 2O 3 : kinetic, isotherm, thermodynamic and mechanism study. Arabian J. Sci. Eng. 43, 3611–3620. https://doi.org/10.1007/s13369-018-3124-3.

Bradford-Hartke, Z., Razmjou, A., Gregory, L., 2021. Factors affecting phosphorus recovery as struvite: effects of alternative magnesium sources. Desalination 504, 114949.

Buates, J., Imai, T., 2020. Biochar functionalization with layered double hydroxides composites: preparation, characterization, and application for effective phosphate removal. J. Water Process Eng. 37, 101508.

Cha-Umpong, W., Dong, G., Razmjou, A., Chen, V., 2019. Effect of oscillating temperature and crystallization on graphene oxide composite pervaporation membrane for inland brine desalination. J. Membr. Sci. 588, 117210.

Chen, M., Huo, C., Li, Y., Wang, J., 2016. Selective adsorption and efficient removal of phosphate from aqueous medium with graphene-lanthanum composite. ACS Sustain. Chem. Eng. 4, 1296–1302. https://doi.org/10.1021/acssuschemeng.5b01324.

Chen, X., Wang, X.C., Yang, S., 2017. La(III) coagulated graphene oxide for phosphate binding: mechanism and behaviour. Int. J. Environ. Stud. 74, 586–602. https://doi.org/10.1080/00207233.2017.1333271.

Chinnathambi, A., Alahmadi, T.A., 2021. Facile synthesis of Fe3O4 anchored polyaniline intercalated graphene oxide as an effective adsorbent for the removal of hexavalent chromium and phosphate ions. Chemosphere 272, 129851.

Delgadillo-Velasco, L., Hernández-Montoya, V., Ramírez-Montoya, L.A., Montes-Morán, M.A., del Rosario Moreno-Virgen, M., Rangel-Vázquez, N.A., 2021. Removal of phosphate and aluminum from water in single and binary systems using iron-modified carbons. J. Mol. Liq. 323, 114586. https://doi.org/10.1016/j.molliq.2020.114586.

Diamadopoulos, E., Benedek, A., 1984. The precipitation of phosphorus from wastewater through pH variation in the presence and absence of coagulants. Water Res. 18, 1175–1179.

Fakhri, A., 2017. Adsorption characteristics of graphene oxide as a solid adsorbent for aniline removal from aqueous solutions: kinetics, thermodynamics and mechanism studies. J. Saudi Chem. Soc. 21, S52–S57.

Gamshadzehi, E., Nassiri, M., Ershadifar, H., 2019. One-pot synthesis of microporous Fe2O3/g-C3N4 and its application for efficient removal of phosphate from sewage and polluted seawater. Colloids Surfaces A Physicochem. Eng. Asp. 567, 7–15.

Gu, Y., Yang, M., Wang, W., Han, R., 2019. Phosphate adsorption from solution by zirconium-loaded carbon nanotubes in batch mode. J. Chem. Eng. Data 64, 2849–2858.

Günther, S., Grunert, M., Müller, S., 2018. Overview of recent advances in phosphorus recovery for fertilizer production. Eng. Life Sci. 18, 434–439.

Han, T., Lu, X., Sun, Y., Jiang, J., Yang, W., Jönsson, P.G., 2020. Magnetic bio-activated carbon production from lignin via a streamlined process and its use in phosphate removal from aqueous solutions. Sci. Total Environ. 708, 135069.

Harijan, D.K.L., Chandra, V., 2017. Akaganeite nanorods decorated graphene oxide sheets for removal and recovery of aqueous phosphate. J. Water Process Eng. 19, 120–125. https://doi.org/10.1016/j.jwpe.2017.07.019.
Hassandoost, R., Pouran, S.R., Khataee, A., Orooji, Y., Joo, S.W., 2019. Hierarchically structured ternary heterojunctions based on Ce3+/Ce4+ modified Fe3O4 nanoparticles anchored onto graphene oxide sheets as magnetic visible-light-active photocatalysts for decontamination of oxytetracycline. J. Hazard Mater. 376, 200–211.
Hassani, A., Khataee, A.R., 2021. Carbon nanomaterials for removal of pharmaceuticals from wastewater. Book Chapter in: Nanomaterials for Water Treatment and Remediation. Taylor and Francis Group, USA (in press).
Hassani, A., Khataee, A.R., 2017. Activated carbon fiber for environmental protection. Activated Carbon Fiber and Textiles. Elsevier, pp. 245–280.
Heidarizadeh, M., Doustkhah, E., Rostamnia, S., Rezaei, P.F., Harzevili, F.D., Zeynizadeh, B., 2017. Dithiocarbamate to modify magnetic graphene oxide nanocomposite (Fe3O4-GO): a new strategy for covalent enzyme (lipase) immobilization to fabrication a new nanobiocatalyst for enzymatic hydrolysis of PNPD. Int. J. Biol. Macromol. 101, 696–702.
Huang, Y., Lee, X., Grattieri, M., Macazo, F.C., Cai, R., Minteer, S.D., 2018. A sustainable adsorbent for phosphate removal: modifying multi-walled carbon nanotubes with chitosan. J. Mater. Sci. 53, 12641–12649.
Huong, P.T., Jitae, K., Giang, B.L., Nguyen, T.D., Thang, P.Q., 2019. Novel lanthanum-modified activated carbon derived from pine cone biomass as ecofriendly bio-sorbent for removal of phosphate and nitrate in wastewater. Rendiconti Lincei. Sci. Fis. Nat. 30, 637–647.
Jiao, G.J., Ma, J., Li, Y., Jin, D., Guo, Y., Zhou, J., Sun, R., 2021. Enhanced adsorption activity for phosphate removal by functional lignin-derived carbon-based adsorbent: optimization, performance and evaluation. Sci. Total Environ. 761 https://doi.org/10.1016/j.scitotenv.2020.143217.
Jun, T.-S., Park, N.-H., So, D.-S., Lee, J.-W., Shim, K.B., Ham, H., 2013. Phosphate removing by graphene oxide in aqueous solution. J. Korean Cryst. Growth Cryst. Technol. 23, 325–328. https://doi.org/10.6111/jkcgct.2013.23.6.325.
Kalderis, D., Koutoulakis, D., Paraskeva, P., Diamadopoulos, E., Otal, E., del Valle, J.O., Fernández-Pereira, C., 2008. Adsorption of polluting substances on activated carbons prepared from rice husk and sugarcane bagasse. Chem. Eng. J. 144, 42–50.
Kalderis, D., Tsuchiya, S., Phillipou, K., Paschalidou, P., Pashalidis, I., Tashima, D., Tsubota, T., 2020. Utilization of pine tree biochar produced by flame-curtain pyrolysis in two non-agricultural applications. Bioresour. Technol. Reports 9, 100384.
Karthikeyan, P., Meenakshi, S., 2020. Enhanced removal of phosphate and nitrate ions by a novel ZnFe LDHs-activated carbon composite. Sustain. Mater. Technol. 25, e00154.
Karthikeyan, P., Meenakshi, S., 2019. Synthesis and characterization of Zn–Al LDHs/activated carbon composite and its adsorption properties for phosphate and nitrate ions in aqueous medium. J. Mol. Liq. 296, 111766.
Karthikeyan, P., Sirajudheen, P., Nikitha, M.R., Meenakshi, S., 2020a. Removal of phosphate and nitrate via a zinc ferrite@ activated carbon hybrid composite under batch experiments: study of isotherm and kinetic equilibriums. Environ. Nanotechnology, Monit. Manag. 14, 100378.
Karthikeyan, P., Vigneshwaran, S., Meenakshi, S., 2020b. Removal of phosphate and nitrate ions from water by amine crosslinked magnetic banana bract activated carbon and its physicochemical performance. Environ. Nanotechnology, Monit. Manag. 13, 100294.
Khalil, A.M.E., Eljamal, O., Amen, T.W.M., Sugihara, Y., Matsunaga, N., 2017. Optimized nano-scale zero-valent iron supported on treated activated carbon for enhanced nitrate and phosphate removal from water. Chem. Eng. J. 309, 349–365.
Khataee, A.R., Aber, S., Zarei, M., Sheydaei, M., 2011. Environmental Applications of Activated Carbon and Carbon Nanotubes. NOVA Science Publisher, Inc., USA (Chapter 1) in Activated Carbon: Classifications, Properties and Applications.
Khataee, A., Hasanzadeh, A., 2017. Modified cathodes with carbon-based nanomaterials for electro-Fenton process. Electro-Fenton Process. Springer, pp. 111–143.
Khodadadi, M., Hosseinnejad, A., Rafati, L., Dorri, H., Nasseh, N., 2017. Removal of phosphate from aqueous solutions by iron nano-magnetic particle coated with powder activated carbon. J. Heal. Sci. Technol. 1, 17–22.
Kilpimaa, S., Runtti, H., Kangas, T., Lassi, U., Kuokkanen, T., 2015. Physical activation of carbon residue from biomass gasification: novel sorbent for the removal of phosphates and nitrates from aqueous solution. J. Ind. Eng. Chem. 21, 1354–1364.
Kilpimaa, S., Runtti, H., Kangas, T., Lassi, U., Kuokkanen, T., 2014. Removal of phosphate and nitrate over a modified carbon residue from biomass gasification. Chem. Eng. Res. Des. 92, 1923–1933.
Koilraj, P., Sasaki, K., 2017. Selective removal of phosphate using La-porous carbon composites from aqueous solutions: batch and column studies. Chem. Eng. J. 317, 1059–1068.
Köksoy, B., Akyüz, D., Şenocak, A., Durmuş, M., Demirbas, E., 2021a. Sensitive, simple and fast voltammetric determination of pesticides in juice samples by novel BODIPY-phthalocyanine-SWCNT hybrid platform. Food Chem. Toxicol. 147, 111886.
Köksoy, B., Akyüz, D., Şenocak, A., Durmuş, M., Demirbaş, E., 2021b. Novel SWCNT-hybrid nanomaterial functionalized with subphthalocyanine substituted asymmetrical zinc (II) phthalocyanine conjugate: design, synthesis, characterization and sensor properties for pesticides. Sensor. Actuator. B Chem. 329, 129198.
Kumar, P., Sudha, S., Chand, S., Srivastava, V.C., 2010. Phosphate removal from aqueous solution using coir-pith activated carbon. Separ. Sci. Technol. 45, 1463–1470.
Kumar, P.S., Prot, T., Korving, L., Keesman, K.J., Dugulan, I., van Loosdrecht, M.C.M., Witkamp, G.-J., 2017. Effect of pore size distribution on iron oxide coated granular activated carbons for phosphate adsorption–Importance of mesopores. Chem. Eng. J. 326, 231–239.
Labgairi, K., Borji, A., Kaddami, M., Jourani, A., 2020. Kinetic study of calcium phosphate precipitation in the system H3PO4-Ca (OH) 2-H2O at 30° C. Int. J. Chem. Eng. 2020.
Lee, J.-H., Velmurugan, P., Ravi, A.V., Oh, B.-T., 2020. Green and hydrothermal assembly of reduced graphene oxide (rGO)-coated ZnO and Fe hybrid nanocomposite for the removal of nitrate and phosphate. Environ. Chem. Ecotoxicol. 2, 141–149. https://doi.org/10.1016/j.enceco.2020.08.001.
Li, J., Fang, X., Yang, M., Tan, W., Zhang, H., Zhang, Y., Li, G., Wang, H., 2020a. The adsorption properties of functionalization vetiver grass-based activated carbon: the simultaneous adsorption of phosphate and nitrate. Environ. Sci. Pollut. Res. 1–11.
Li, T., Lü, S., Wang, Z., Huang, M., Yan, J., Liu, M., 2021. Lignin-based nanoparticles for recovery and separation of phosphate and reused as renewable magnetic fertilizers. Sci. Total Environ. 765 https://doi.org/10.1016/j.scitotenv.2020.142745.
Li, X., Elgarhy, A.H., Hassan, M.E., Chen, Y., Liu, G., ElKorashey, R., 2020b. Removal of inorganic and organic phosphorus compounds from aqueous solution by ferrihydrite decoration onto graphene. Environ. Monit. Assess. 192 https://doi.org/10.1007/s10661-020-08325-y.
Liu, J., Wan, L., Zhang, L., Zhou, Q., 2011. Effect of pH, ionic strength, and temperature on the phosphate adsorption onto lanthanum-doped activated carbon fiber. J. Colloid Interface Sci. 364, 490–496.
Liu, J., Xia, S., Lü, X., Shen, H., 2017. Adsorption of tricresyl phosphate onto graphene nanomaterials from aqueous solution. Water Sci. Technol. 76, 1565–1573. https://doi.org/10.2166/wst.2017.317.
Liu, J., Zhou, Q., Chen, J., Zhang, L., Chang, N., 2013. Phosphate adsorption on hydroxyl–iron–lanthanum doped activated carbon fiber. Chem. Eng. J. 215, 859–867.
Liu, L., Huang, G., Song, P., Yu, Y., Fu, S., 2016a. Converting industrial alkali lignin to biobased functional additives for improving fire behavior and smoke suppression of polybutylene succinate. ACS Sustain. Chem. Eng. 4, 4732–4742. https://doi.org/10.1021/acssuschemeng.6b00955.
Liu, L., Qian, M., Song, P., Huang, G., Yu, Y., Fu, S., 2016b. Fabrication of green lignin-based flame retardants for enhancing the thermal and fire retardancy properties of polypropylene/wood composites. ACS Sustain. Chem. Eng. 4, 2422–2431. https://doi.org/10.1021/acssuschemeng.6b00112.
Liu, R., Hao, X., Chen, Q., Li, J., 2019a. Research advances of Tetrasphaera in enhanced biological phosphorus removal: a review. Water Res. 166, 115003.
Liu, X., Fu, J., Tang, Y., Smith Jr., R.L., Qi, X., 2021. Mg-coordinated self-assembly of MgO-doped ordered mesoporous carbons for selective recovery of phosphorus from aqueous solutions. Chem. Eng. J. 406, 126748.
Liu, X., He, X., Zhang, J., Yang, J., Xiang, X., Ma, Z., Liu, L., Zong, E., 2020. Cerium oxide nanoparticle functionalized lignin as a nano-biosorbent for efficient phosphate removal. RSC Adv. 10, 1249–1260. https://doi.org/10.1039/c9ra09986g.
Liu, Xiaoning, Shen, F., Smith Jr., R.L., Qi, X., 2019b. Black liquor-derived calcium-activated biochar for recovery of phosphate from aqueous solutions. Bioresour. Technol. 294, 122198.
Liu, Xiaohuan, Zong, E., Hu, W., Song, P., Wang, J., Liu, Q., Ma, Z., Fu, S., 2019c. Lignin-derived porous carbon loaded with La(OH) 3 nanorods for highly efficient removal of phosphate. ACS Sustain. Chem. Eng. 7, 758–768. https://doi.org/10.1021/acssuschemeng.8b04382.
Liu, Z., Wu, W., Liu, Y., Hu, X., 2018. Preparation of surface anion imprinted polymer by developing a La(III)-coordinated 3-methacryloxyethyl-propyl bi-functionalized graphene oxide for phosphate removal. J. Taiwan Inst. Chem. Eng. 85, 282–290. https://doi.org/10.1016/j.jtice.2018.02.001.
Luedecke, C., Hermanowicz, S.W., Jenkins, D., 1988. Precipitation of ferric phosphate in activated sludge: a chemical model and its verification. Water Pollution Research and Control Brighton. Elsevier, pp. 325–337.
Luo, X., Liu, C., Yuan, J., Zhu, X., Liu, S., 2017. Interfacial solid-phase chemical modification with Mannich reaction and Fe(III) chelation for designing lignin-based spherical nanoparticle adsorbents for highly efficient removal of low concentration phosphate from water. ACS Sustain. Chem. Eng. 5, 6539–6547. https://doi.org/10.1021/acssuschemeng.7b00674.
Luo, X., Wang, X., Bao, S., Liu, X., Zhang, W., Fang, T., 2016. Adsorption of phosphate in water using one-step synthesized zirconium-loaded reduced graphene oxide. Sci. Rep. 6, 1–13. https://doi.org/10.1038/srep39108.
Mahdavi, S., Akhzari, D., 2016. The removal of phosphate from aqueous solutions using two nano-structures: copper oxide and carbon tubes. Clean Technol. Environ. Policy 18, 817–827.
Makita, Y., Sonoda, A., Sugiura, Y., Ogata, A., Suh, C., Lee, J., Ooi, K., 2019. Preparation and phosphate adsorptive properties of metal oxide-loaded granular activated carbon and pumice stone. Colloids Surfaces A Physicochem. Eng. Asp. 582, 123881.
Manjunath, S.V., Kumar, M., 2018. Evaluation of single-component and multi-component adsorption of metronidazole, phosphate and nitrate on activated carbon from Prosopıs juliflora. Chem. Eng. J. 346, 525–534.
Marshall, J.A., Morton, B.J., Muhlack, R., Chittleborough, D., Kwong, C.W., 2017. Recovery of phosphate from calcium-containing aqueous solution resulting from biochar-induced calcium phosphate precipitation. J. Clean. Prod. 165, 27–35.
Mathieux, F., Ardente, F., Bobba, S., Nuss, P., Blengini, G.A., Dias, P.A., Blagoeva, D., de Matos, C.T., Wittmer, D., Pavel, C., 2017. Critical Raw Materials and the Circular Economy. Publ. Off. Eur. Union Luxemb.
Mayer, B.K., Baker, L.A., Boyer, T.H., Drechsel, P., Gifford, M., Hanjra, M.A., Parameswaran, P., Stoltzfus, J., Westerhoff, P., Rittmann, B.E., 2016. Total value of phosphorus recovery. Environ. Sci. Technol. 50, 6606–6620.
Mekonnen, D.T., Alemayehu, E., Lennartz, B., 2020. Removal of phosphate ions from aqueous solutions by adsorption onto leftover coal. Water 12, 1381.

Miyazato, T., Nuryono, N., Kobune, M., Rusdiarso, B., Otomo, R., Kamiya, Y., 2020. Phosphate recovery from an aqueous solution through adsorption-desorption cycle over thermally treated activated carbon. J. Water Process Eng. 36, 101302.
Mohammadi, R., Hezarjaribi, M., Ramasamy, D.L., Sillanpää, M., Pihlajamäki, A., 2021. Application of a novel biochar adsorbent and membrane to the selective separation of phosphate from phosphate-rich wastewaters. Chem. Eng. J. 407, 126494.
Mojoudi, N., Soleimani, M., Mirghaffari, N., Belver, C., Bedia, J., 2019. Removal of phenol and phosphate from aqueous solutions using activated carbons prepared from oily sludge through physical and chemical activation. Water Sci. Technol. 80, 575–586.
Monser, L., Adhoum, N., 2002. Modified activated carbon for the removal of copper, zinc, chromium and cyanide from wastewater. Separ. Purif. Technol. 26, 137–146.
Mor, S., Chhoden, K., Negi, P., Ravindra, K., 2017. Utilization of nano-alumina and activated charcoal for phosphate removal from wastewater. Environ. Nanotechnology, Monit. Manag. 7, 15–23.
Najmi, S., Hatamipour, M.S., Sadeh, P., Najafipour, I., Mehranfar, F., 2020. Activated carbon produced from Glycyrrhiza glabra residue for the adsorption of nitrate and phosphate: batch and fixed-bed column studies. SN Appl. Sci. 2, 1–22.
Nakarmi, A., Bourdo, S.E., Ruhl, L., Kanel, S., Nadagouda, M., Alla, P.K., Pavel, I., Viswanathan, T., 2020. Benign zinc oxide betaine-modified biochar nanocomposites for phosphate removal from aqueous solutions. J. Environ. Manag. 272, 111048.
Namasivayam, C., Sangeetha, D., 2004. Equilibrium and kinetic studies of adsorption of phosphate onto ZnCl2 activated coir pith carbon. J. Colloid Interface Sci. 280, 359–365.
Nguyen, T.M.P., Van, H.T., Nguyen, T.V., Ha, L.T., Vu, X.H., Pham, T.T., Nguyen, T.N., Quang, N.V., Nguyen, X.C., 2020. Phosphate adsorption by silver nanoparticles-loaded activated carbon derived from tea residue. Sci. Rep. 10, 1–13.
Orooji, Y., Ghanbari Gol, H., Jaleh, B., Rashidian Vaziri, M.R., Eslamipanah, M., 2021. Large optical nonlinearity of the activated carbon nanoparticles prepared by laser ablation. Nanomaterials 11, 737.
Polyakov, M., Ivanova, V., Klyamer, D., Köksoy, B., Şenocak, A., Demirbaş, E., Durmuş, M., Basova, T., 2020a. A hybrid nanomaterial based on single walled carbon nanotubes cross-linked via axially substituted silicon (IV) phthalocyanine for chemiresistive sensors. Molecules 25, 2073.
Polyakov, M.S., Ivanova, V.N., Basova, T.V., Saraev, A.A., Köksoy, B., Şenocak, A., Demirbaş, E., Durmuş, M., 2020b. 3D, covalent and noncovalent hybrid materials based on 3-phenylcoumarin derivatives and single walled carbon nanotubes as gas sensing layers. Appl. Surf. Sci. 504, 144276.
Qiao, X., Liao, S., Zheng, R., Deng, Y., Song, H., Du, L., 2016. Cobalt and nitrogen codoped graphene with inserted carbon nanospheres as an efficient bifunctional electrocatalyst for oxygen reduction and evolution. ACS Sustain. Chem. Eng. 4, 4131–4136.
Rashidi Nodeh, H., Sereshti, H., Zamiri Afsharian, E., Nouri, N., 2017. Enhanced removal of phosphate and nitrate ions from aqueous media using nanosized lanthanum hydrous doped on magnetic graphene nanocomposite. J. Environ. Manag. 77 (3), 252–266. https://doi.org/10.1016/j.jenvman.2017.04.004.
Razmjou, A., Hosseini, E., Cha-Umpong, W., Korayem, A.H., Asadnia, M., Moazzam, P., Orooji, Y., Karimi-Maleh, H., Chen, V., 2020. Effect of chemistry and geometry of GO nanochannels on the Li ion selectivity and recovery. Desalination 496, 114729.
Rezaei, H., Rastegar, S., Naseri, S., 2019. Application of chitosan and activated carbon nano-composite in removal of nitrite, phosphate, and ammonia from aquaculture wastewater. Avicenna J. Environ. Heal. Eng. 6, 106–112.
Rostamnia, S., Doustkhah, E., Karimi, Z., Amini, S., Luque, R., 2015. Surfactant-exfoliated highly dispersive Pd-supported graphene oxide nanocomposite as a catalyst for aerobic aqueous oxidations of alcohols. ChemCatChem 7, 1678–1683.
Safarpour, M., Khataee, A., 2019. Graphene-based materials for water purification. Nanoscale Materials in Water Purification. Elsevier, pp. 383–430.
Safarpour, M., Khataee, A., Vatanpour, V., 2015. Thin film nanocomposite reverse osmosis membrane modified by reduced graphene oxide/TiO2 with improved desalination performance. J. Membr. Sci. 489, 43–54.
Safarpour, M., Vatanpour, V., Khataee, A., 2016. Preparation and characterization of graphene oxide/TiO2 blended PES nanofiltration membrane with improved antifouling and separation performance. Desalination 393, 65–78.
Sakamoto, T., Amano, Y., Machida, M., 2020. Phosphate ion adsorption properties of PAN-based activated carbon fibers prepared with K 2 CO 3 activation. SN Appl. Sci. 2, 1–8.
Sakulpaisan, S., Vongsetskul, T., Reamouppaturm, S., Luangkachao, J., Tantirungrotechai, J., Tangboriboonrat, P., 2016. Titania-functionalized graphene oxide for an efficient adsorptive removal of phosphate ions. J. Environ. Manag. 92 (12), 3049–3057. https://doi.org/10.1016/j.jenvman.2015.11.028.
Salehi, S., Hosseinifard, M., 2020. Optimized removal of phosphate and nitrate from aqueous media using zirconium functionalized nanochitosan-graphene oxide composite. Cellulose 27, 8859–8883. https://doi.org/10.1007/s10570-020-03382-5.
Sarıoğulları, H., Şenocak, A., Basova, T., Demirbaş, E., Durmuş, M., 2019. Effect of different SWCNT-BODIPY hybrid materials for selective and sensitive electrochemical detection of guanine and adenine. J. Electroanal. Chem. 840, 10–20.
Sarvajayakesavalu, S., Lu, Y., Withers, P.J.A., Pavinato, P.S., Pan, G., Chareonsudjai, P., 2018. Phosphorus recovery: a need for an integrated approach. Ecosys. Health Sustain. 4, 48–57.
Şenocak, A., Khataee, A., Demirbas, E., Doustkhah, E., 2020. Ultrasensitive detection of rutin antioxidant through a magnetic micro-mesoporous graphitized carbon wrapped Co nanoarchitecture. Sensor. Actuator. B Chem. 312, 127939.
Şenocak, A., Tümay, S.O., Makhseed, S., Demirbas, E., Durmuş, M., 2021. A synergetic and sensitive physostigmine pesticide sensor using copper complex of 3D zinc (II) phthalocyanine-SWCNT hybrid material. Biosens. Bioelectron. 174, 112819.
Sereshti, H., Zamiri Afsharian, E., Esmaeili Bidhendi, M., Rashidi Nodeh, H., Afzal Kamboh, M., Yilmaz, M., 2020. Removal of phosphate and nitrate ions aqueous using strontium magnetic graphene oxide nanocomposite: isotherms, kinetics, and thermodynamics studies. Environ. Prog. Sustain. Energy 39, 1–12. https://doi.org/10.1002/ep.13332.
Seviour, R.J., Mino, T., Onuki, M., 2003. The microbiology of biological phosphorus removal in activated sludge systems. FEMS Microbiol. Rev. 27, 99–127.
Shan, S., Tang, H., Zhao, Y., Wang, W., Cui, F., 2019. Highly porous zirconium-crosslinked graphene oxide/alginate aerogel beads for enhanced phosphate removal. Chem. Eng. J. 359, 779–789. https://doi.org/10.1016/j.cej.2018.10.033.
Shindo, T., Takao, Y., Ikeuchi, T., Ozawa, S., 2011. Adsorption of phosphate from aqueous solutions onto zirconium loaded activated carbons derived from lignocellulosic residues. Int. J. Soc. Mater. Eng. Resour. 18, 24–31.
Singh, A.K., Singh, K.P., 2018. Optimization of phosphate removal from aqueous solution using activated carbon supported zero-valent iron nanoparticles: application of RSM approach. Appl. Water Sci. 8, 1–9.
Smol, M., 2019. The importance of sustainable phosphorus management in the circular economy (CE) model: the Polish case study. J. Mater. Cycles Waste Manag. 21, 227–238.
Sowmya, A., Meenakshi, S., 2013. An efficient and regenerable quaternary amine modified chitosan beads for the removal of nitrate and phosphate anions. J. Environ. Chem. Eng. 1, 906–915.
Sreekumar, U., Thalla, A.K., Nair, V.V., 2019. Comparative evaluation of phosphate abatement using laterite soil and activated carbon. Int. J. Environ. Sci. Technol. 16, 4493–4502.
Sujitha, R., Ravindhranath, K., 2017. Extraction of phosphate from polluted waters using calcium alginate beads doped with active carbon derived from A. aspera plant as adsorbent. J. Anal. Methods Chem. 2017.
Tahmasebi, E., 2020. Insights into the adsorption mechanism of Al30 polyoxocations-modified graphene oxide nanosheets for efficient removal of phosphate, chromate and selenate oxyanions: a comparative study. J. Mol. Liq. 299 https://doi.org/10.1016/j.molliq.2019.112111.
Thakur, S., Govender, P.P., Mamo, M.A., Tamulevicius, S., Mishra, Y.K., Thakur, V.K., 2017. Progress in lignin hydrogels and nanocomposites for water purification: future perspectives. Vacuum 146, 342–355. https://doi.org/10.1016/j.vacuum.2017.08.011.
Tran, D.N.H., Kabiri, S., Wang, L., Losic, D., 2015. Engineered graphene-nanoparticle aerogel composites for efficient removal of phosphate from water. J. Mater. Chem. 3, 6844–6852. https://doi.org/10.1039/c4ta06308b.
Vasudevan, S., Lakshmi, J., 2012. The adsorption of phosphate by graphene from aqueous solution. RSC Adv. 2, 5234–5242. https://doi.org/10.1039/c2ra20270k.
Veni, D.K., Kannan, P., Edison, T.N.J.I., Senthilkumar, A., 2017. Biochar from green waste for phosphate removal with subsequent disposal. Waste Manag. 68, 752–759.
Vera-Puerto, I., Saravia, M., Olave, J., Arias, C., Alarcon, E., Valdes, H., 2020. Potential application of Chilean natural zeolite as a support medium in treatment wetlands for removing ammonium and phosphate from wastewater. Water 12, 1156.
Vicente-Martínez, Y., Caravaca, M., Soto-Meca, A., De Francisco-Ortiz, O., Gimeno, F., 2020. Graphene oxide and graphene oxide functionalized with silver nanoparticles as adsorbents of phosphates in waters. A comparative study. Sci. Total Environ. 709, 136111.
Wajima, T., 2016. Phosphate adsorption on zirconium-loaded activated carbon, and its application for phosphate recovery from deep seawater. Int. J. Chem. Eng. Appl. 7, 388.
Wan, X., Khan, M.A., Wang, F., Xia, M., Lei, W., Zhu, S., Fu, C., Ding, Y., 2019. Facile synthesis of protonated g-C3N4 and acid-activated montmorillonite composite with efficient adsorption capacity for PO43− and Pb (II). Chem. Eng. Res. Des. 152, 95–105.
Wang, B., Lian, G., Lee, X., Gao, B., Li, L., Liu, T., Zhang, X., Zheng, Y., 2020. Phosphogypsum as a novel modifier for distillers grains biochar removal of phosphate from water. Chemosphere 238, 124684.
Wang, B., Wen, J.L., Sun, S.L., Wang, H.M., Wang, S.F., Liu, Q.Y., Charlton, A., Sun, R.C., 2017a. Chemosynthesis and structural characterization of a novel lignin-based bio-sorbent and its strong adsorption for Pb (II). Ind. Crop. Prod. 108, 72–80. https://doi.org/10.1016/j.indcrop.2017.06.013.
Wang, H., Zhang, P., Liu, J., 2017b. Triethylene tetramine functionalized magnetic graphene oxide chitosan composite with superior capacity for the removal of phosphate. J. Chem. Eng. Data 62, 3341–3352. https://doi.org/10.1021/acs.jced.7b00417.
Wang, Y., Li, Z., Wang, J., Li, J., Lin, Y., 2011. Graphene and graphene oxide: biofunctionalization and applications in biotechnology. Trends Biotechnol. 29, 205–212.
Wang, Y., Yang, Q., Huang, H., 2019. Effective adsorption of trace phosphate and aluminum in realistic water by carbon nanotubes and reduced graphene oxides. Sci. Total Environ. 662, 1003–1011.
Wang, Z., Nie, E., Li, J., Yang, M., Zhao, Y., Luo, X., Zheng, Z., 2012. Equilibrium and kinetics of adsorption of phosphate onto iron-doped activated carbon. Environ. Sci. Pollut. Res. 19, 2908–2917.
Wang, Z., Shi, M., Li, J., Zheng, Z., 2014. Influence of moderate pre-oxidation treatment on the physical, chemical and phosphate adsorption properties of iron-containing activated carbon. J. Environ. Sci. 26, 519–528.
WHO, 2018. WHO Global Water, Sanitation and Hygiene 2018–2019.
Xiong, W., Tong, J., Yang, Z., Zeng, G., Zhou, Y., Wang, D., Song, P., Xu, R., Zhang, C., Cheng, M., 2017. Adsorption of phosphate from aqueous solution using iron-zirconium modified activated carbon nanofiber: performance and mechanism. J. Colloid Interface Sci. 493, 17–23.

Xu, X., Song, W., Huang, D., Gao, B., Sun, Y., Yue, Q., Fu, K., 2015. Performance of novel biopolymer-based activated carbon and resin on phosphate elimination from stream. Colloids Surfaces A Physicochem. Eng. Asp. 476, 68–75.
Xuechu, C., Hainan, K., Deyi, W.U., Xinze, W., Yongyong, L.I.N., 2009. Phosphate removal and recovery through crystallization of hydroxyapatite using xonotlite as seed crystal. J. Environ. Sci. 21, 575–580.
Yao, S., Wang, M., Liu, J., Tang, S., Chen, H., Guo, T., Yang, G., Chen, Y., 2018. Removal of phosphate from aqueous solution by sewage sludge-based activated carbon loaded with pyrolusite. J. Water Reuse Desalin. 8, 192–201.
Yin, Q., Wang, R., Zhao, Z., 2018. Application of Mg–Al-modified biochar for simultaneous removal of ammonium, nitrate, and phosphate from eutrophic water. J. Clean. Prod. 176, 230–240.
Zaytseva, O., Neumann, G., 2016. Carbon nanomaterials: production, impact on plant development, agricultural and environmental applications. Chem. Biol. Technol. Agric. 3, 1–26. https://doi.org/10.1186/s40538-016-0070-8.
Zhang, L., Gao, Y., Zhou, Q., Kan, J., Wang, Y., 2014. High-performance removal of phosphate from water by graphene nanosheets supported lanthanum hydroxide nanoparticles. Water, Air, Soil Pollut. 225 https://doi.org/10.1007/s11270-014-1967-0.
Zhang, L., Liu, J., Wan, L., Zhou, Q., Wang, X., 2012a. Batch and fixed-bed column performance of phosphate adsorption by lanthanum-doped activated carbon fiber. Water, Air, Soil Pollut. 223, 5893–5902.
Zhang, L., Wang, Z., Xu, X., Chen, C., Gao, B., Xiao, X., 2019a. Insights into the phosphate adsorption behavior onto 3D self-assembled cellulose/graphene hybrid nanomaterials embedded with bimetallic hydroxides. Sci. Total Environ. 653, 897–907.
Zhang, L., Zhou, Q., Liu, J., Chang, N., Wan, L., Chen, J., 2012b. Phosphate adsorption on lanthanum hydroxide-doped activated carbon fiber. Chem. Eng. J. 185, 160–167.
Zhang, Z., Yan, L., Yu, H., Yan, T., Li, X., 2019b. Adsorption of phosphate from aqueous solution by vegetable biochar/layered double oxides: fast removal and mechanistic studies. Bioresour. Technol. 284, 65–71.
Zhang, Z., Yi, L.I., Leilei, W.E.I., Yufeng, L.Ü., Meng, W., Baoyu, G.A.O., 2013. Effect of ferric chloride on the properties of biological sludge in co-precipitation phosphorus removal process. Chin. J. Chem. Eng. 21, 564–568.
Zhao, Y., Shan, X., An, Q., Xiao, Z., Zhai, S., 2020. Interfacial integration of zirconium components with amino-modified lignin for selective and efficient phosphate capture. Chem. Eng. J. 398, 1–10. https://doi.org/10.1016/j.cej.2020.125561.
Zong, E., Huang, G., Liu, X., Lei, W., Jiang, S., Ma, Z., Wang, J., Song, P., 2018. A lignin-based nano-adsorbent for superfast and highly selective removal of phosphate. J. Mater. Chem. 6, 9971–9983. https://doi.org/10.1039/c8ta01449c.
Zong, E., Liu, X., Jiang, J., Fu, S., Chu, F., 2016. Preparation and characterization of zirconia-loaded lignocellulosic butanol residue as a biosorbent for phosphate removal from aqueous solution. Appl. Surf. Sci. 387, 419–430. https://doi.org/10.1016/j.apsusc.2016.06.107.
Zong, E., Liu, X., Wang, J., Yang, S., Jiang, J., Fu, S., 2017. Facile preparation and characterization of lanthanum-loaded carboxylated multi-walled carbon nanotubes and their application for the adsorption of phosphate ions. J. Mater. Sci. 52, 7294–7310.
Zong, E., Wei, D., Wan, H., Zheng, S., Xu, Z., Zhu, D., 2013. Adsorptive removal of phosphate ions from aqueous solution using zirconia-functionalized graphite oxide. Chem. Eng. J. 221, 193–203. https://doi.org/10.1016/j.cej.2013.01.088.